Zeitschrift: IABSE congress report = Rapport du congrès AIPC = IVBH Kongressbericht

Band: 9 (1972)

Rubrik: Theme V: Tall slender structures

V
Bâtiments hauts élancés
Hohe schlanke Bauwerke
Tall Slender Structures

Leere Seite
Blank page
Page vide

V

Dynamic Design of High-Rise Building subjected to Wind and Seismic Loads

Projet d'une structure élevée soumise aux charges dynamiques du vent et des séismes

Entwurf eines Hochbaues unter Berücksichtigung von dynamischen Wind- und Erdbebenkräften

MASAYOSHI KAWAMURA
Eng. D., Struc. Engr.

KAZUO WAKABAYASHI
Struc. Engr.

Nikken Sekkei Ltd, Japan

SHIZUO BAN
Eng. D., Prof. Emeritus

TAKUJI KOBORI
Eng. D., Prof.

Kyoto University, Japan

1. Introduction

The structural design of a high-rise building should be based on the different design principle depending on whether the building should be designed for wind load only or for wind load together with the effect of destructive earthquake. If the former is just the case, the greater the lateral stiffness of the building, the better the building for structural safety, whereas in the latter case, the increased stiffness causes a greater storey shear force to act on the building during an earthquake and is therefore often undesirable.

In a high-rise building for which seismic load is under prime consideration, the design is characterized by design conditions necessary for such a building and by structural solutions pertinent to such design conditions. Of a number of solutions that can be considered for the foregoing problem, the case of the KTC Building (The Kobe, Commerce, Industry and Trade Center Building, Kobe, Japan) is reported in this paper. The structural design for this building was accomplished in October 1967 and its construction was completed in October 1969.

2. Outline of the KTC Building

The KTC Building structure consists of a perimeter composed of a framed tube structure and a core consisting of braced rigid frames. As a structural solution for such a centre-cored high-rise building, this system can offer a number of advantages both for structural and economical problems. Figs. 1 and 2 show the typical plan and section of the KTC Building.

A framed tube structure used in the perimeter of a high-rise building essentially results in a very narrow width available for doorways at the ground floor level, and this gives rise to a problem to which a proper solution must be given.

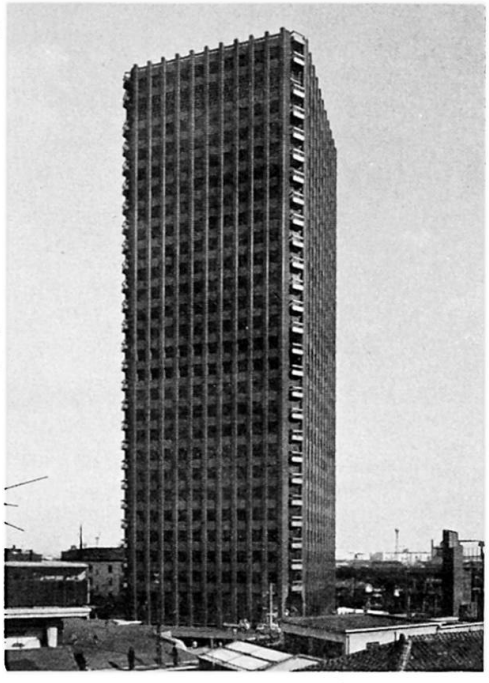

KTC BLDG. (Kobe, Japan)

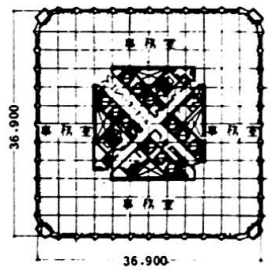

Fig.1 Typical plan

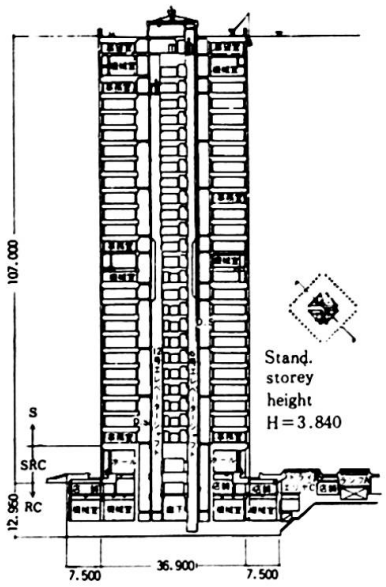

Fig. 2 Section

In this building, the problem is solved by locating the main doorways at each corner of the perimeter where the column spacing is wider than elsewhere. This also makes it possible to carry out the column spacing on upper storeys down to the ground floor without modification of the continuous framework and is therefore considered an advantageous approach to the solution of this kind of problem. As a result of the foregoing doorway locations, the beams in the core structure are placed diagonally across the building, thereby serving to insure the horizontal rigidity of the core slab that has many through-floor opening space such as elevator shafts and stairways.

The structural system of this building is shown in Figs. 3 and 4. The structural design is featured by the following:

a. The favourable minimum lateral stiffness of the building is given to resist wind force.

b. The building is based on the dynamic design through the iteration of earthquake response analyses to resist seismic force.

c. The structure is designed as a three-dimensional frame, consisting of the perimeter frame and cored frame, capable of resisting the foregoing lateral force.

d. Efforts are made to give the framework continuity of stiffness, required strength and sufficient ductility.

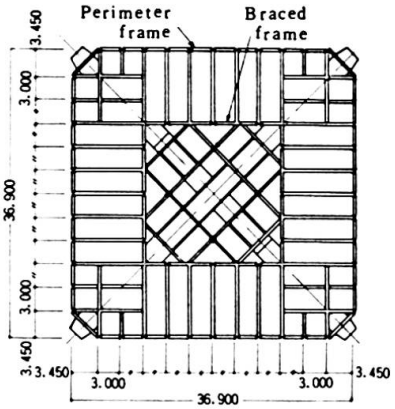

Fig. 3 Beam plan

e. The framework is designed in such a way that the yielding of members would occur in the beams and not in the columns or braces in the case of over-loading.

f. The basement and the ground floor are constructed of the reinforced concrete and steel-frame reinforced concrete respectively to be sufficiently rigid so as to satisfy the assumption of the fixed base for the upper storey in the response analyses.

g. The steel-frame reinforced concrete construction is adopted for the ground floor in order to avoid the abrupt stiffness change from the upper storeys to the basement.

h. The steel construction is adopted for the second to the top floors so as to reduce the weight of the building structure. The qualities and thickness-to-width restrictions imposed on the principal members are given in Table 1.

i. Both partitions and exterior walls are designed to minimize the weight of the building and also to be acceptable for such deflections as may be

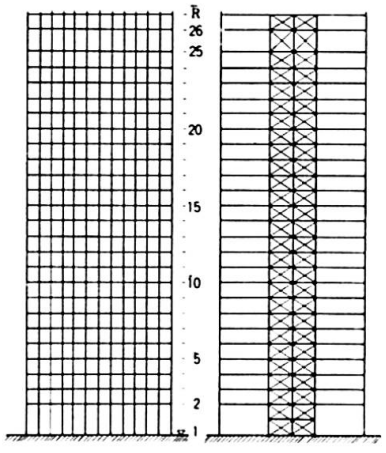

Fig. 4 Structural system

caused during a great earthquake.

3. Aseismic Design

3.1 Design Procedure

The aseismic design procedure adopted for the KTC Building is as shown by the following chart:

Table 1 Materials

Member	Section	Quality	Max. b/t	
Column	rolled H (series 400)	SM50A SM50B	flange web	8 37
Beam (primary)	built-up H	SM41	flange web	9 50
Beam (secondary)	built-up H rolled H honeycomb H	SM41 SS41	flange web	15 71
Brace	bar	Gr. 4	—	

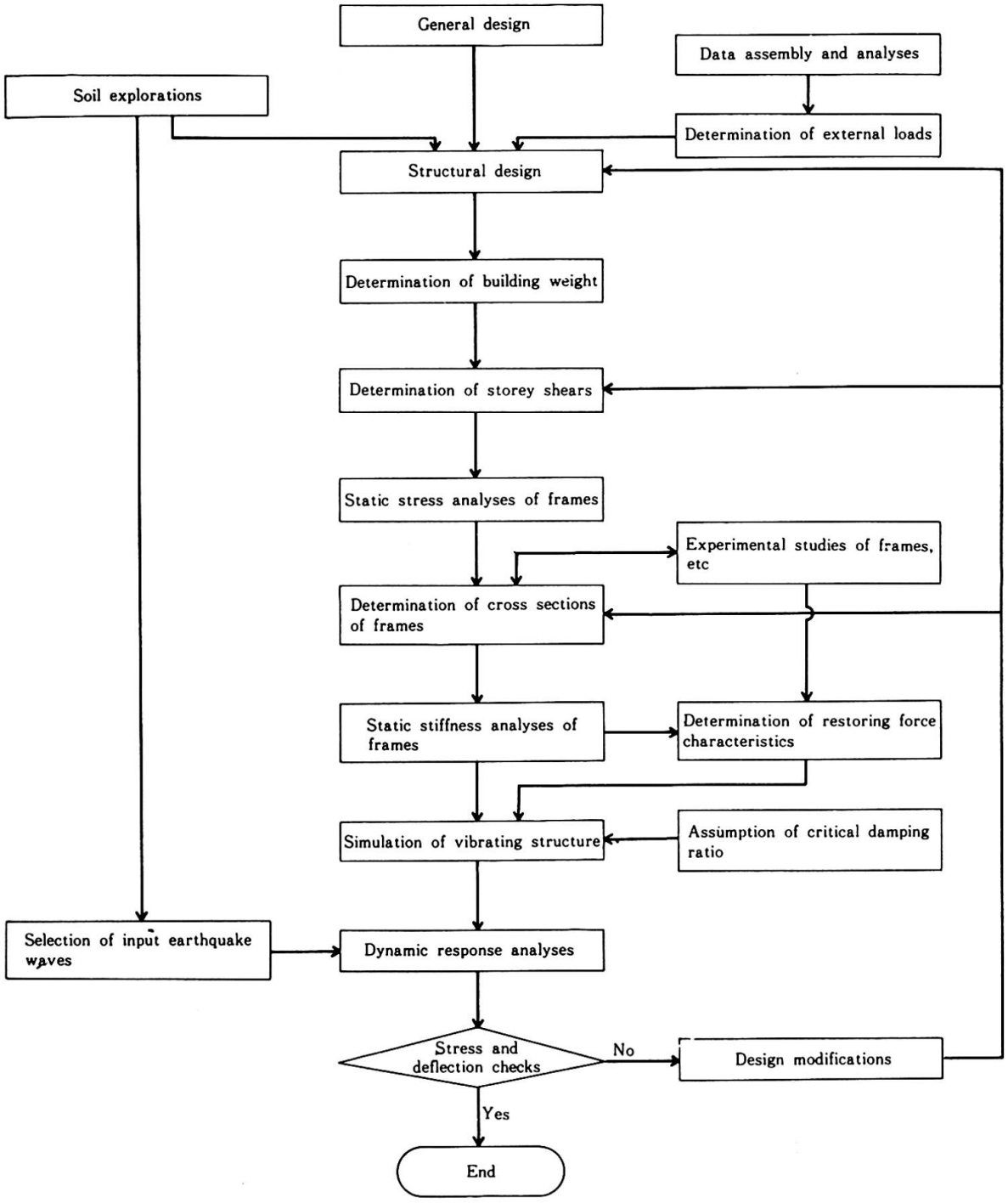

3.2 Basic Equation

The equation used in the dynamic analysis is written as follows:

$$[M]\{\ddot{y}\} + [C]\{\dot{y}\} + [K]\{y\} = -[M]\{\ddot{y}_o\}$$

where, $[M]$ = Mass matrix
$[C]$ = Damping matrix
$[K]$ = Stiffness matrix
$\{y\}$ = Relative displacement vector
$\{y_o\}$ = Ground displacement vector

3.3 Seismic Force and Permissible Storey Deflection

The input waves of earthquake ground motions adopted for this analysis are as shown in Figs. 14 and 15. As to the anticipated intensity of earthquakes, the maximum acceleration value of ground motions is estimated as 200 - 300 gals, because the maximum value of the greatest earthquake occurred in Kobe area was less than 100 gals in the past. Against these earthquake ground motions permissible deflection for each storey of the building is restricted to $h_i/200$ approximately (where h_i represents each storey height) so that stresses in all members would be within the elastic range. In addition, the elasto-plastic responses are analized with respect to earthquake motions with the maximum acceleration value of 400 gals. Since the natural period of a building often tends to be shorter than the computed period, the response characteristics are also studied in the case of the fundamental period which is assumed as 0.9 or 0.8 times the value of the computed natural period.

The seismic force used for the structural design is shown in Fig. 5. To evaluate this design seismic force, firstly the storey shears corresponding to the structural responses to the aforesaid ground motions are obtained through the iteration of response analyses for the case of the maximum acceleration value and the critical damping ratio assumed as 200 (300) gals and 2% respectively. Secondly, the storey shears thus obtained are plotted on a graph and an envelope embracing such plotted shears is evaluated finally as the applicable seismic force.

3.4 Wind Force and Permissible Storey Deflection

The design wind force to be assumed as a static external force is derived from the following formula:

$$P = C \cdot q \cdot A$$

where, C = Wind force coefficient (in this case, $C = 1.10$)
q = Velocity pressure expressed as $q_o \cdot \sqrt[4]{h/10}$ (in this case, $q_o = 175$ kg/m^2)
A = Area exposed to wind force

In this formula, the value of q_o is determined on the basis of the typhoons recorded in Kobe area in the past and the value of C, by a wind tunnel test of a model. The favourable minimum lateral stiffness of the building is determined in such a way that stresses in all the members would be within an elastic range, that the maximum deflection at the top of the building would not exceed H/400 (where H = the building height), and that the maximum storey deflection would be not

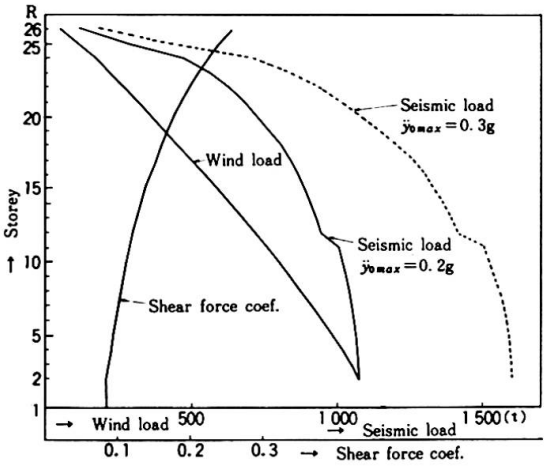

Fig. 5 Design loads

more than $h_i/300$ all under the foregoing wind force. The design wind force is shown in Fig. 5. The total wind force thus obtained is approximately equal to the base shear force caused by an earthquake ground motion where its acceleration value is taken as 200 gals.

3.5 Stiffness Distribution

The magnitude of earthquake response is governed by the characteristics of earthquakes and the dynamic properties (mainly dependent on mass and lateral stiffness distribution, i.e., natural periods and modes of vibration) of the building structure. While the structural engineer has little freedom in selecting the mass distribution, he can choose the desirable stiffness distribution more freely.

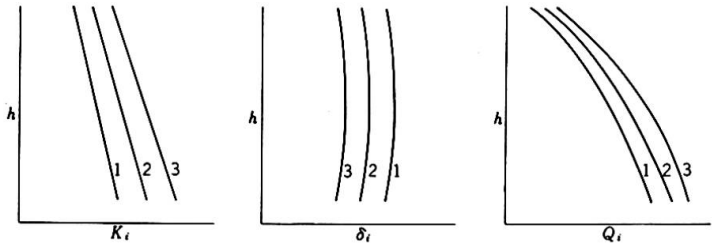

Fig. 6 General relationship between stiffness and response

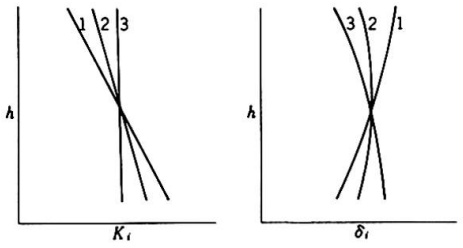

Fig. 7 General relationship between stiffness and storey deflection

In the first place, it may be stated that the shear force generally tends to increase as the stiffness of a structure increases (or in other words as its natural periods decrease). On the contrary, the shear force decreases as the stiffness becomes small or as the natural periods become great. In this case, however, the horizontal deflection of the building increases. Fig. 6 shows a general tendency of the relationship mentioned above.

Secondly, it is known that lateral stiffness distribution in direction of the height of a building affects deflection distribution in that building. Each storey deflection should be made as uniform as possible throughout the height of a building; however, the stiffness must be adequately distributed in direction of the height of a building in order to achieve this purpose satisfactorily. Fig. 7 shows the general tendency of this relationship.

It is pointed out that the aseismic design requirement for a structure remarkably differs from the ordinary lateral force design as shown in Figs. 6 and 7. For instance, a heavily braced frame increases the stiffness of a building and enables it to favourably resist overturning moment at a reasonable cost, and is, therefore, satisfactory for a wind-resistant structure. Such a frame, however, often turns out to be undesirable for an earthquake-resistant structure, because it usually gives a building too large stiffness distributed as shown in curve 1 of Fig. 7.

In the structural design of the KTC Building, high strength steel bars are used for bracings. The purpose of such bracings is to optimize the stiffness distribution in direction of the height without increasing adversely the

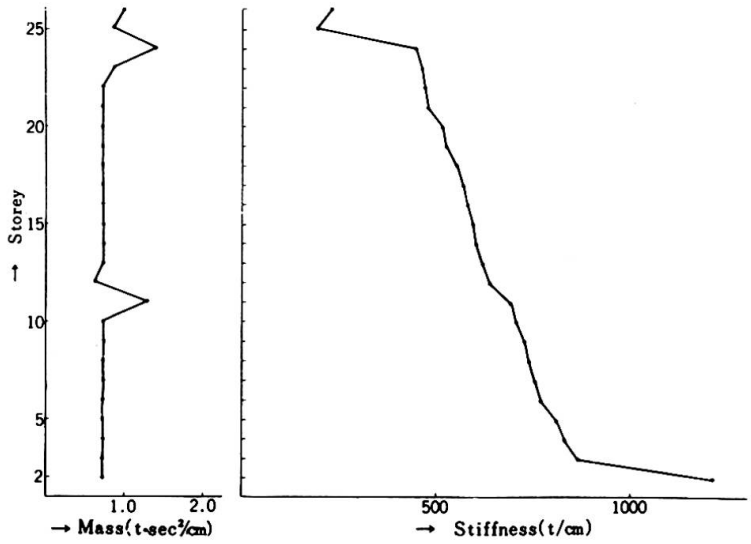

Fig. 8 Mass and stiffness distribution

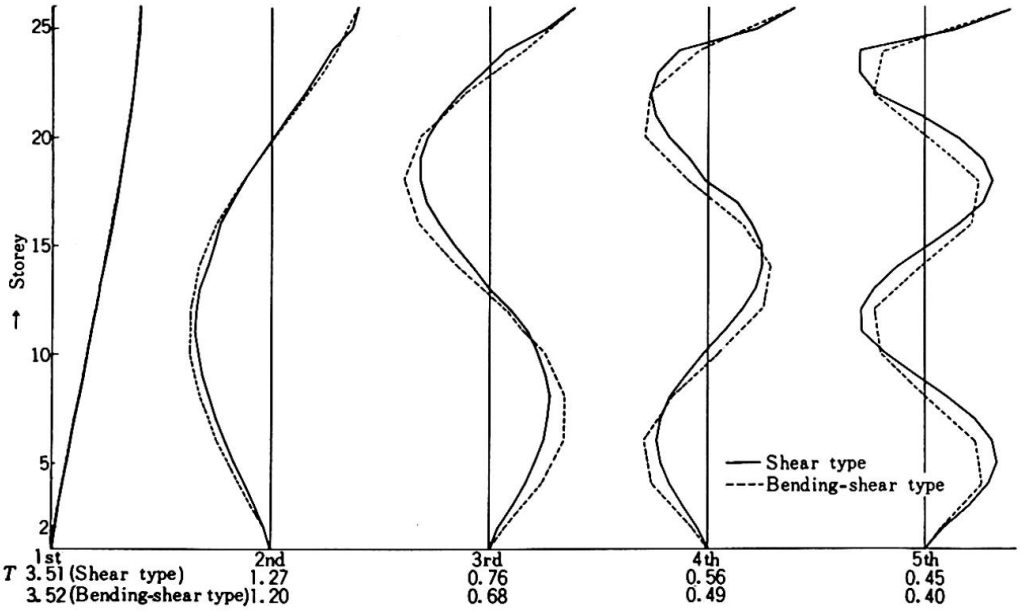

Fig. 9 Modes of vibrations and natural periods

stiffness of the building as a whole and to sufficiently enlarge the elastic range of the bracings. These braces are capable of deforming within an elastic range under a storey deflection up to 4 cm approximately.

Fig. 8 shows the mass distribution and the stiffness distribution (under the shear type vibration) as computed for a simulated model of the KTC Building idealized by the lumped mass system. The earthquake responses of such a model are shown in Figs. 11 through 13. The stiffness distribution as shown in Fig. 8 ensures the response deflection which is approximately made uniform through all storeys within an allowable limit. Table 2 shows the computed natural periods for the building as completed (without live loads) and for the building as occupied (with live loads). Fig. 9 shows each mode of vibration to which the building under occupancy would be subjected.

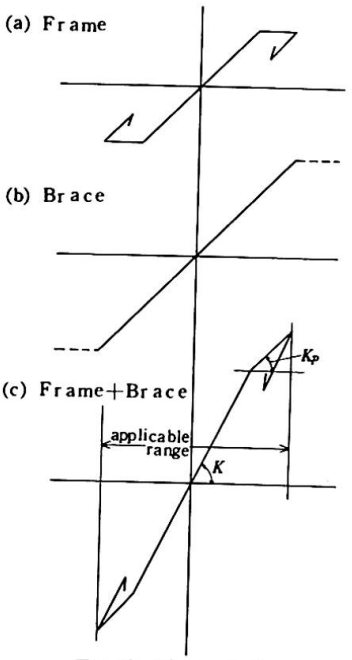

Fig. 10 Elasto-plastic restoring force characteristic

3.6 Results of Analyses

Some results of the earthquake responses analyses are shown in Figs. 11 - 14. Fig. 11 indicates the vibration of simulated model of the building idealized

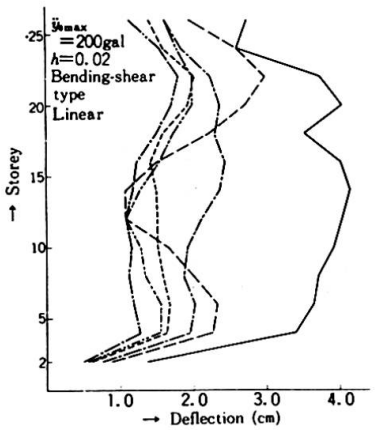

Fig. 12 Deflection in earthquake response

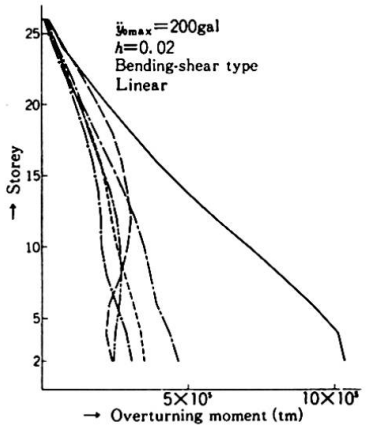

Fig. 13 Max. overturning moment in earthquake response

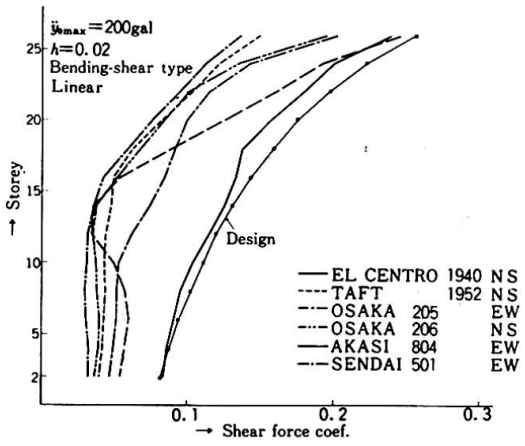

Fig. 14 Max. shear force coef. in earthquake response

Table 2 Natural periods

Vibration type	Assumed condition	$_1T$	$_2T$	$_3T$	$_4T$	$_5T$
Shear type	Before occupancy	3.51	1.27	0.76	0.56	0.45
Bending-shear type	Before occupancy	3.52	1.20	0.68	0.49	0.40
	After occupancy	3.33	1.14	0.64	0.46	0.37

by the lumped mass system as related to time lapse during earthquakes. Figs. 12 and 13 show the deflection and the maximum overturning moment in earthquake responses respectively. Fig. 14 indicates the maximum shear force coefficient computed from earthquake responses. The ductility factors corresponding to various input earthquake waves are shown in Fig. 15. In these analyses, every two storeys are considered one lumped mass except for Fig. 11 in which each storey is considered one lumped mass. The elasto-plastic restoring force characteristics of the framework are assumed, as a whole, to be bi-linear as shown in Fig. 10. From these results, it is known that the earthquake responses largely depend on the patterns of input earthquake waves. The maximum storey deflection is within h/200 - h/250, the permissible deflection range, under the maximum acceleration amplitude of 200 gals of input waves. Some portions of the frame structure are in a plastic range under El Centro 1940 (NS component) of the maximum acceleration amplitude in excess of 300 gals. However, the ductility factors are not more than 1.2 and 2.0 under the maximum acceleration values of 300 gals and 400 gals respectively. In studies with regard to the other wave patterns it is found that the responses remain in elastic range under the maximum acceleration amplitude of about 500 gals.

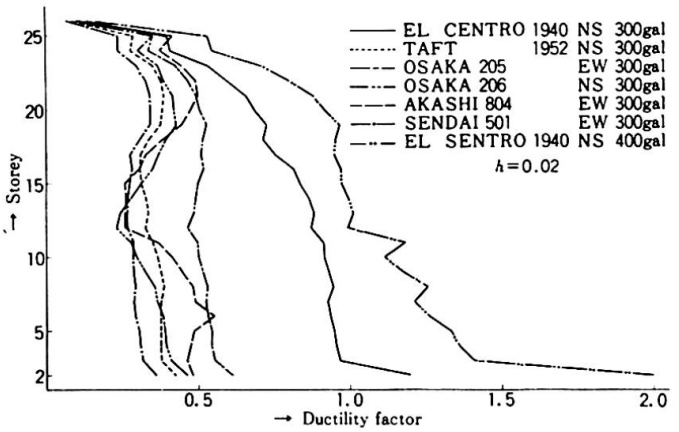

Fig. 15 Distribution of ductility factor

Table 3 Strength and stiffness under wind load

Storey	Storey shear (t)	Stiffness for wind load K=(t/cm)	Max-deflection in elastic range δ_{Yi} (cm)	Max-storey deflection δ_i (cm)	h/δ_i	δ_i/δ_{Yi}
26	46.6	186.4	9.70	0.25	1540	0.03
25	109.1	170.5	6.94	0.64	900	0.09
24	170.6	370.9	4.60	0.46	830	0.10
23	219.2	405.9	4.14	0.54	710	0.13
22	267.3	431.1	4.04	0.62	620	0.15
21	314.8	449.7	3.94	0.70	550	0.18
20	361.8	488.9	3.74	0.74	520	0.20
19	408.3	510.4	3.62	0.80	480	0.22
18	454.2	540.7	3.65	0.84	460	0.23
17	499.5	561.2	3.61	0.89	430	0.25
16	544.2	572.8	3.56	0.95	400	0.27
15	588.2	594.1	3.59	0.99	390	0.28
14	631.4	607.1	3.55	1.04	370	0.29
13	673.8	623.9	3.52	1.08	360	0.31
12	715.5	650.5	3.53	1.10	350	0.31
11	756.5	694.0	3.29	1.09	350	0.33
10	796.6	717.7	3.26	1.11	350	0.34
9	835.7	739.6	3.18	1.12	340	0.36
8	873.8	753.3	3.10	1.16	330	0.37
7	910.8	765.4	3.13	1.19	320	0.38
6	946.5	782.2	3.07	1.21	320	0.39
5	980.8	824.2	2.92	1.19	320	0.41
4	1,013.7	844.8	2.89	1.20	320	0.42
3	1,044.8	870.7	2.78	1.20	320	0.43
2	1,073.8	1.234	1.81	0.87	440	0.48

$\delta_{top} = \Sigma\delta_i = 22.83\,\text{cm} \fallingdotseq H/460$

The results of wind load analysis as shown in Table 3 indicate that the storey deflection at lower storeys is about h/320 or about 40% of the maximum deformation in an elastic range. The maximum deflection at the top of the building is approximately h/460 corresponding to the sufficient stiffness of the frame against the wind load.

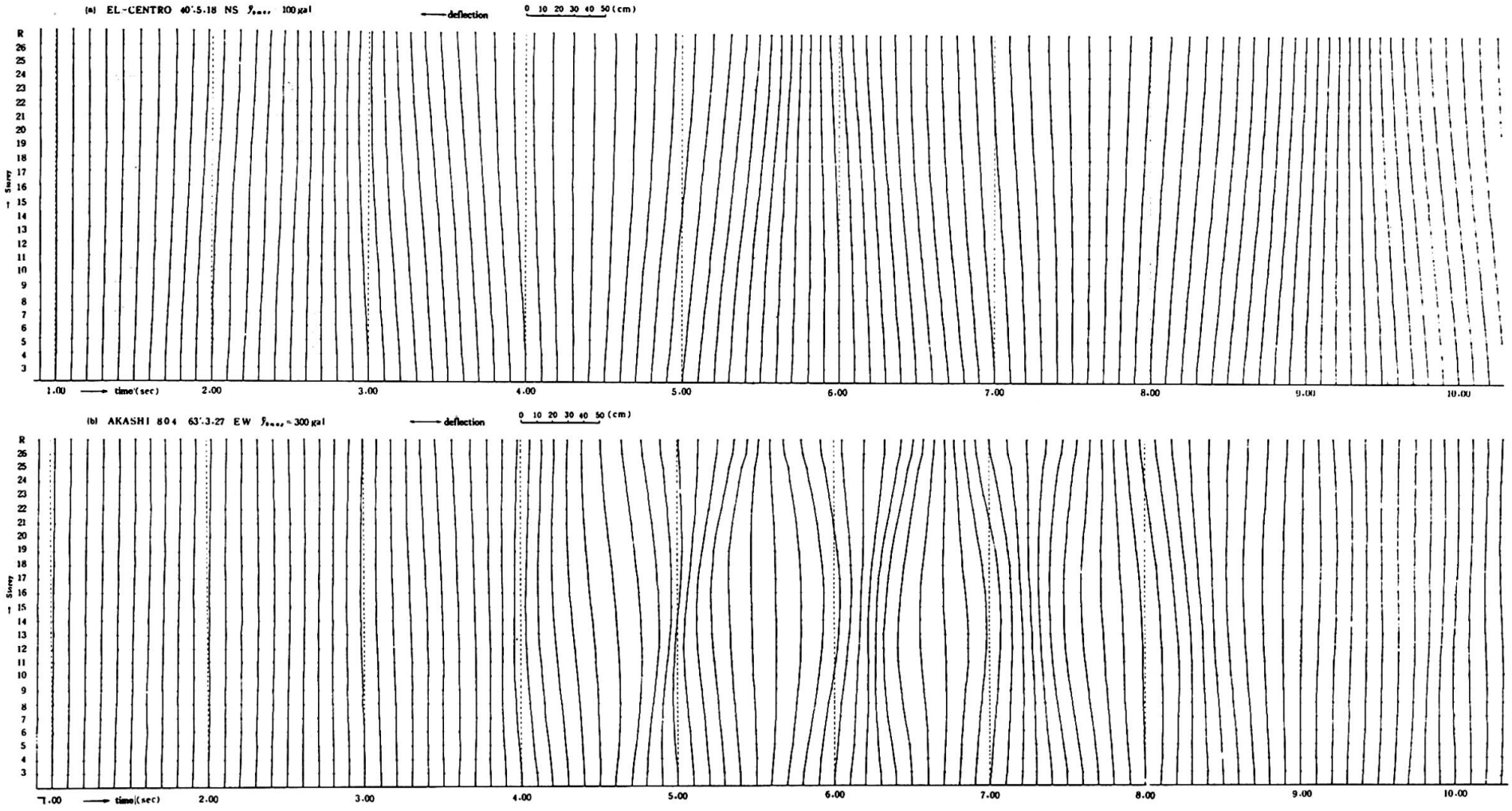

Fig. 11 Simulated vibration of the building

4. Vibration Tests

4.1 Test Procedure

When the building was under construction, its vibration characteristics were ascertained by such experimental approaches as forced vibration tests and micro-tremor measurements, and these experimental results were compared with the dynamic characteristics computed by means of theoretical analyses. The vibration tests consisted of the preliminary and main tests, and the main tests were carried out twice, first upon the completion of the framework and the second when the exterior and interior wall coverings had been placed.

For these tests, the excitation was effected by means of a pendulum and an oscillator located at the centre of the core. The excited storeys are shown in Table 4. The excitation by pendulum was intended to generate the fundamental mode of vibration, and for this purpose, a pendulum weighing 5 tons was suspended from the beams of the 25th floor. The oscillator was of eccentric mass type with maximum excitation capacity for 2 tons, and it was used to generate the 2nd to 5th modes of vibration of the building.

Table 4 Excitation procedures and excited storeys

Test	Procedures	E-W direction		N-S direction	
		$_1T$	$_2T \sim _5T$	$_1T$	$_2T \sim _5T$
Preliminary test	Micro-tremors				
1st and 2nd test	Micro-tremors				
	By pendulum	25F		25F	
	By oscillator		26F, 14F		26F

4.2 Test Results

Table 5 shows some of test results. As can be seen from the table, the measured values of the natural periods are about 75% of those obtained through theoretical analysis. The measured natural periods obtained under micro-tremors coincide considerably well with those recorded under forced vibration. In this case the critical damping ratio does not exceed 1% under lower order vibrations of the building.

4.3 Discussion

The difference between theoretical and measured values of natural periods is largely attributable to the fact that the stiffness of the structure is evaluated on a different basis. In this connection, the following findings are made:

(1) As high strength steel bars are slightly pre-tensioned, the bracings on compression side as well as tension side can contribute to the stiffness

Table 5 Results of vibration test

Tests	Natural periods			$_1T$	$_2T$	$_3T$	$_4T$	$_5T$
Preliminary test	Computed values		T	2.21	0.80	0.49	0.35	0.27
	Measured values	Micro-tremors	T	1.73	0.65	0.40	0.28	0.21
1st test	Computed values		T	3.04	1.08	0.62	0.44	0.35
		*	T'	2.77	0.93	0.52	0.37	0.30
	Measured values	Micro-tremors	T	2.25	0.80	0.44	0.32	0.25
		Forced vibration	T	2.26	0.80	0.45	0.32	0.25
			h	0.50	0.53	0.95	1.80	2.20
2nd test	Computed values		T	3.33	1.14	0.64	0.46	0.37
		*	T'	3.04	0.97	0.54	0.39	0.31
	Measured values	Forced vibration	T	2.51	0.82	0.43	0.31	0.22
			h	0.87	1.28	2.40	2.1	2.9

* T': modified values as mentioned in (4.3)

of the building under the small amplitude of vibration.

(2) Concrete floor slabs are integrated with beams by means of stud connectors to produce composite effects.

(3) Splice plates used for field connections of beams and columns increase the effective stiffness of the members concerned.

(4) Gussets for brace connection help expand the zone of stiffness under bending moments.

(5) No analysis is made as to the framework at the central core, located at an angle of 45° with respect to the principal frames, comprising four columns because its influence on the building stiffness is very small.

(6) Exterior and interior walls are so detailed as to be separated from the principal structural frames; however, it is easily considered that they contribute to the stiffness of the building under small amplitude of vibration.

Of the foregoing findings, effects described in Subparagraphs (1) through (5) are taken into consideration and then the natural periods are re-computed accordingly. The modified values thus obtained are shown in Table 5. The ratio of the measured values to the modified values is about 82%, which is considered to be very satisfactory when compared with the difference between theoretical and measured values for similar experiments in the past. In making structural analyses of high-rise construction, the effects as described above must be considered.

Bibliography

(1) Leonhardt, F. : High-Rise Slender Building : Introductory Report, 9th Congr. IABSE, Amsterdam 1972, pp. 233-237.

(2) Wakabayashi, K., Kawamura, M., Ban, S., Yamada, M. : Bracing System composed of High-Strength Steel Bars as adopted in Aseismic Design of a High-Rise Building : Preliminary Publication, 9th Congr. IABSE, Amsterdam 1972.

(3) Khan, F. R. : Column-Free Box-Type Framing with and without Core : Preliminary Publication, 8th Congr. IABSE, New York, 1968, pp. 261-273.

(4) Ban, S., Kobori, T., Yamada, M., Kawamura, M., Wakabayashi, K. : Researches on the Structural Design of the KTC BLDG. : Annual Convention of the Architectural Institute of Japan, August 1969, pp. 1105-1118.

Summary

In the structural design of high-rise building, lateral stiffness of framework and its distribution in direction of the height of building must be given an essential consideration because the earthquake response characteristics of the building are greatly affected by these two important stiffness assessments. In stiffness computation, every computable factor which affects the structural behaviours should be taken into consideration.

A structural system consisting of rigid perimeter frames as well as of frames braced by high strength steel, so designed as to form a three-dimensional space structure, is believed to offer highly effective solution for the structural safety.

V

Hull-Core Structures subjected to Bending and Torsion

Eléments hull-core soumis à la flexion et à la torsion

Hull-core Elemente beansprucht durch Biegung und Torsion

A. COULL N.K. SUBEDI
Department of Civil Engineering
University of Strathclyde
Glasgow, Scotland

1. Introduction

During the past few years a number of new structural systems have been developed for high-rise buildings. A natural evolution of the familiar rigidly-jointed frame which has been used increasingly is the rigid box or tube type of system [1]. This form consists essentially of four orthogonal frame panels forming in plan a framed tube (cf. Fig. 1). Each panel consists of a number of exterior columns connected by stiff spandrel beams at each floor level. Although the exterior 'perforated tube' may be used solely to resist all wind forces, it is commonly designed to act in conjunction with an inner core to form a hull-core or tube-in-tube system. This inner core, which may be used to contain all building services, will consist of some combination of beams, columns, shear walls and box elements surrounding lift shafts and stair wells. The open area between the outer frame and inner core allows flexibility in layout planning. The system has been employed for both steel and concrete construction.

The behaviour of a perforated tube is more complex than that of a simple closed-tube, and the stiffness is less. In addition to the cantilever bending action, which produces tensile and compressive stresses on opposite faces of the tube, the side frames undergo the usual plane-frame shearing action in each storey. The primary action is complicated by the fact that the flexibility of the spandrel beams produces a shear lag which has the effect of increasing the stresses in the corner columns, and reducing them in the inner columns of the normal panels. The latter effects will produce warping of the floor slabs and consequent deformations of interior partitions and secondary structure.

The inclusion of an inner core which is connected to the outer hull by moment-resistant members will have the effect of inducing axial forces in the columns of the normal panels, which will tend to offset the reduction of stresses caused by shear lag. However, it appears to be more economic to use simply supported floor systems which do not resist lateral forces; for this reason, the floor system can be relatively shallow, and longer spans can be used between the outer and inner structures.

It is important to be able to assess both the warping effect and the amount of sway produced by lateral forces, since either may control the design of the structure. The object of the present paper is to demonstrate how the analysis of the complex three-dimensional structure may be simplified through a recognition of the dominant structural actions, particular attention being paid to the torsional behaviour. In addition, experimental results from tests on model structures are presented to show the different modes of behaviour of framed-tube, hull-core, and unperforated tube structures.

2. Analysis

Consider the hull-core structural system of Fig. 1 subjected to some lateral loading. It is assumed that the floor system is so stiff in its own plane that all cross-sections of the building undergo only rigid body movements in plan. Any applied load may then be considered equivalent to the superposition of a bending force and a torsional moment referred to the centre of rotation. If the behaviour of the structure is elastic, the two may be treated independently.

Since the overall action is complex, it is advantageous to consider the action of the outer tube alone before examining the composite hull-core interaction.

2.1 Outer Tube

(i) Bending action.

In a framed-tube subjected to bending by lateral forces, (cf. Fig. 1) the loads are resisted by two primary actions - the axial deformations of the normal panels (AB and CD) and the racking actions in the side panels (AD and BC). The primary interactive forces between the normal and side panels will be vertical (shear) forces transmitted through the corner columns. Secondary out-of-plane deformations will occur, but it is assumed that these will be restricted sufficiently by the high in-plane stiffness of the floor system to be neglible in comparison with the primary effects. All individual elements will then deflect equally at each floor level.

By assuming this dominant mode of deformation, the three-dimensional frame may be replaced by the equivalent plane frame shown in Fig. 2. It is assumed that, as is generally the case, the structure is symmetrical about both centre-lines so that only one-quarter (FDE) need be considered in the analysis, the appropriate joint conditions on the centre-lines being as indicated. The high in-plane stiffness of the floor system allows the horizontal forces at each floor level to be applied in the plane of the side frames (Fig. 2).

It is desired to transmit only vertical forces between side and normal panels, whilst maintaining conditions of compatibility at the corner. This may be achieved very simply in a normal plane frame analysis by the use of fictitious 'vertical shea transfer' beams DD′ (Fig. 2) at each floor level. In the stiffness matrix for the fictitious beams, the shear elements must be made a very large quantity, (relative to the elements in the stiffness matrices for the real members) with all other elements zero [2]. In practice, it has been found that a value of around 10^4 times the largest element gives the desired transfer. The corner columns can be considered to contribute half their cross-sectional areas to each panel, together with their appropriate second moment of area in each orthogonal direction.

From the frame analysis, the flexibility matrix $\underset{\sim}{F}_H$ may be determined to give the relationship between applied loads and the resulting horizontal deflections,

$$\underset{\sim}{Y}_H = \underset{\sim}{F}_H \underset{\sim}{P}_H \qquad (1)$$

where $\underset{\sim}{Y}_H$ and $\underset{\sim}{P}_H$ are column vectors of the horizontal deflections and applied horizontal forces at each storey level.

The accuracy of the technique was checked by comparing the results obtained for a number of plane and space frames with those from standard computer programmes. In one typical test, the six-storey structure shown in plan in Fig. 3 was chosen, this being the largest configuration which could be solved by the available program within the given constraints. The section properties of the columns and spandrel beams were as follows: columns - 8 in x 8 in x 58 lb; I_{xx} = 227.3 in^4; I_{yy} = 74.9 in^4; A = 17.06 in^2; J = 3.37 in^4; beams - 5 in x 12 in x 31.8 lb; I_{xx} = 215.8 in^4; I_{yy} = 9.5 in^4, A = 9.26 in^2; J = 0.92 in^4. The storey height was maintained constant at 12 ft. The results obtained from the two analyses are

compared in Tables 1 and 2, the latter giving deflections throughout the height, and the former axial forces and bending moments at the most heavily loaded first storey level. The results refer to a unit load (1 ton) at each floor level.

Column	Space Frame Analysis			Simplified Method		
	Axial Force	Bending Moment (ton in)		Axial Force	Bending Moment (ton in)	
	(ton)	Lower End	Upper End	(ton)	Lower End	Upper End
1	0	-93.9	-84.1	0	-97.5	-87.4
2	+0.16	-188.6	-169.8	+0.19	-195.9	-176.6
3	-21.51	-167.2	-127.0	-10.90	-173.9	-132.5
3′		-2.68	-5.13	-10.90	-2.65	-5.14
4	-3.63	-2.42	-4.65	-3.66	-2.39	-4.66
5	-0.97	-0.63	-1.15	-0.97	-0.60	-1.12
6	-0.30	-0.15	-0.26	-0.30	-0.14	-0.25

Table 1. Axial Forces and Bending Moments in First Storey Columns.

Storey	1	2	3	4	5	6
Deflection (Space Frame) in.	0.234	0.484	0.695	0.863	0.984	1.058
Deflection (Simplified Method) in.	0.242	0.497	0.711	0.879	0.999	1.072

Table 2. Deflections

The agreement was even better at the upper levels, the axial forces and moments corresponding to within 1% at the third storey level. Small discrepancies will always occur since the three-dimensional analysis does not include the in-plane restraint of the floor slabs.

The accuracy of the simplified techniques has also been demonstrated experimentally[2] .

(ii) Torsional action.

The application of a twisting moment to a framed-tube structure produces two forms of deformation, a pure rotation and an out-of-plane warping displacement of the cross-section. The combined action may be considered as a combination of the plane frame actions of the four panels and the effects of the interactions between the panels. It is again assumed that the floor slabs act as rigid diaphragms so that all structural elements at any cross-section rotate equally under torque. Twisting moments will be resisted primarily by shearing actions in the orthogonal panels, and the torsional moments resisted by individual beam and column elements are assumed negligible. If the rotations are small, the frame panels may be assumed to deform in their own plane.

In Fig. 4, let θ be the rotation of any cross-section of the structure under

the action of an applied torque T. If Δ_1 and Δ_2 are the deflections of panels DC and DA in their own planes, then

$$\theta = \frac{\Delta_1}{c} = \frac{\Delta_2}{b} \qquad (2)$$

For torsional equilibrium,

$$2q_1 c + 2q_2 b = T \qquad (3)$$

where q_1 and q_2 are the horizontal shear forces resisted by panels DC and DA respectively.

Equations corresponding to (2) and (3) may be written for all storey levels and, expressing them in matrix form, the compatibility and equilibrium conditions for the entire structure become,

$$\underset{\sim}{\theta} = \frac{1}{c}\ \underset{\sim}{\Delta}_1 = \frac{1}{b}\ \underset{\sim}{\Delta}_2 \qquad (4)$$

$$2c\ \underset{\sim}{q}_1 + 2b\ \underset{\sim}{q}_2 = \underset{\sim}{T} \qquad (5)$$

where $\underset{\sim}{\theta}$, $\underset{\sim}{\Delta}_1$ and $\underset{\sim}{\Delta}_2$ are column vectors of rotations and horizontal deflections, $\underset{\sim}{T}$ is a vector of total applied twisting moments, and $\underset{\sim}{q}_1$ and $\underset{\sim}{q}_2$ are vectors of the total horizontal forces in the panels, at each floor level.

The panel horizontal displacements may be related to the horizontal shear forces by the relationship

$$\underset{\sim}{\Delta}_1 = \underset{\sim}{F}_1\ \underset{\sim}{q}_1 \qquad \text{and} \qquad \underset{\sim}{\Delta}_2 = \underset{\sim}{F}_2\ \underset{\sim}{q}_2 \qquad (6)$$

where $\underset{\sim}{F}_1$ and $\underset{\sim}{F}_2$ are square matrices of horizontal deflection flexibilities for panels DC and DA, which may be derived from a standard plane frame analysis. When evaluating the flexibility matrices the interactions between orthogonal panels must be included; Fig. 5 indicates the unit forces required for the evaluation of $\underset{\sim}{F}_1$ and $\underset{\sim}{F}_2$ respectively. By this means, both in-plane rotations and out-of-plane warping effects may be included. Again only one-quarter of a symmetrical structure need be included in the analysis, using the appropriate skew-symmetrical boundary conditions at the axes of symmetry.

The matrix of rotations θ may be obtained from equations (4), (5) and (6) to be,

$$\underset{\sim}{\theta} = \left[2c^2\ \underset{\sim}{F}_1^{-1} + 2b^2\ \underset{\sim}{F}_2^{-1} \right]^{-1} \underset{\sim}{T} = \underset{\sim}{F}_3^{-1}\ \underset{\sim}{T} \qquad (7)$$

where $\underset{\sim}{F}_3$ is the torsional flexibility matrix for the outer hull.

The displacements and horizontal forces are obtained from equations (4) and (6) respectively, and all internal stress-resultants follow from the frame analysis.

2.2 Hull-Core Structure

In view of the high in-plane stiffness of the floor slabs, it is assumed that the hull and core are constrained to deflect together in the composite structure. Consequently, under pure bending action, all elements have the same horizontal deflection, whilst under a pure twisting action, the rotations of both hull and core will be equal at each floor level. The two actions may again be considered independently.

(i) Bending action.

If, as is generally the case, the floor structure is designed to be

effectively pin-connected to both hull and core, no moments are transmitted between the two. Under the action of wind forces, the floor system then acts as a rigid pin-ended link transmitting horizontal forces only.

If the applied loads and resulting deflections of the core are related in an analogous manner to equation (1) by a flexibility matrix $\underset{\sim}{F}_c$, then

$$\underset{\sim}{Y}_c = \underset{\sim}{F}_c \underset{\sim}{P}_c \tag{8}$$

The flexibility matrix $\underset{\sim}{F}_c$ may be determined from ordinary beam theory if the inner core can be assumed to act as a pure cantilever. If it consists of an inner framed tube, the method described previously may be used. The continuous connection technique may be utilised to give an assessment of the flexibility of a coupled shear wall core [3].

The conditions of horizontal compatibility and equilibrium at each level are,

$$\underset{\sim}{Y}_c = \underset{\sim}{Y}_H \quad \text{and} \quad \underset{\sim}{P} = \underset{\sim}{P}_H + \underset{\sim}{P}_c \tag{9}$$

where $\underset{\sim}{P}$ is the column vector of resultant wind forces at each floor level.

The solutions of equations (1), (8) and (9) yields the distribution of forces between the hull and core,

$$\begin{aligned} \underset{\sim}{P}_H &= \left[\underset{\sim}{I} + \underset{\sim}{F}_c^{-1} \underset{\sim}{F}_H \right]^{-1} \underset{\sim}{P} \\ \underset{\sim}{P}_c &= \left[\underset{\sim}{I} + \underset{\sim}{F}_H^{-1} \underset{\sim}{F}_c \right]^{-1} \underset{\sim}{P} \end{aligned} \tag{10}$$

Once the distribution of horizontal forces is known, the stress-resultants in the frame panels follow from the frame analysis.

(ii) Torsional action.

The twisting moments and rotations of the inner core will be related by

$$\underset{\sim}{\theta}_c = \underset{\sim}{F}_4 \underset{\sim}{T}_c \tag{11}$$

where $\underset{\sim}{F}_4$ is the matrix of torsional flexibility coefficients. The matrix $\underset{\sim}{F}_4$ may be determined by the technique described earlier if the core consists of an inner framed tube; for thin walled elements, Vlasov's theory of thin walled beams may be used [3], whilst if the core consists of coupled shear-wall elements, the continuous connection method may be utilised to give the flexibility coefficients [3].

The conditions of rotational compatibility and equilibrium then become,

$$\underset{\sim}{\theta} = \underset{\sim}{\theta}_c \quad \text{and} \quad \underset{\sim}{T} = 2c\, \underset{\sim}{q}_1 + 2b\, \underset{\sim}{q}_2 + \underset{\sim}{T}_c \tag{12}$$

The solution of equations (2), (4), (6), (11) and (12) yields the matrix of rotations,

$$\underset{\sim}{\theta} = \left[2c^2 \underset{\sim}{F}_1^{-1} + 2b^2 \underset{\sim}{F}_2^{-1} + \underset{\sim}{F}_4^{-1} \right]^{-1} \underset{\sim}{T} \tag{13}$$

The horizontal shear forces in the outer frame panels and twisting moments in the core follow from equations (4) and (6), and (11) respectively.

The analysis assumes that no torsion coupling of the hull and core occurs through the floor slabs. That is, the floor system is assumed to offer no restraint against warping of either hull or core.

3. Experimental Investigations

In parallel with the theoretical studies, a series of tests was carried out on model framed-tube and hull-core structures, with a view to assessing the accuracy of theoretical predictions and to examining the influence of an inner core on the deformations and stresses in the composite structure.

Experiments were performed on two fifteen-storey perspex models, one with a closed box (torsionally stiff) core and the other with an open channel (torsionally weak) core. The columns for the outer framed tube and the plates for the inner cores were cut from 3/16 in. thick perspex sheet, and the floor slabs from 1/8 in. thick sheet. The hull had eight columns along one side and five along the other, each column being 1/2 in. wide , the corner ones being glued together to form an angle section. The plan dimensions are shown in Fig. 1. The storey height was 2-1/8 in., with a 2 in. clear height between floor slabs. Because of the small size of the models, it was not possible to form the desired hinged connections between vertical and horizontal members, and all joints were glued. The perimeter columns were then connected solely by floor slabs at each floor level, the columns being glued into edge slots in the slabs.

The models were tested initially as framed-tube structures, and subsequently, after inserting and glueing the inner cores into central holes left in the floor slabs, as composite hull-core systems. The inner cores were tested individually to check their calculated bending and torsional stiffnesses. A rigid-base condition was achieved by glueing all columns and cores into slots passing through a one-inch thick perspex base plate. The models were cantilevered horizontally in a test frame, the base being further stiffened by passing steel sections across the base plate as near as possible to the model.

Lateral loads were applied by hanging dead weights from nylon cords at each floor level, deflections and strains being measured by dial gauges and electrical resistance strain gauges, respectively. A concentrated twisting moment was applied at the free end by means of a twelve-inch diameter perspex disc containing a rectangular hole to fit over the end of the model (cf. Fig. 6). Equal and opposite tangential loads were applied at opposite ends of a diameter by dead weights which hung from thin nylon threads passing over pulleys. Similar devices were used to apply twisting moments to the inner cores before they were inserted into the framed-tube models to form hull-core structures. Loads were applied in increments, at fixed time intervals to minimise creep effects, and unit values obtained from the best linear curve of strain or deflection against load.

Separate tests were performed on a representative section of floor slab and columns in order to assess the effective stiffness of the floor slab in connecting the perimeter columns.

In order to compare the mode of behaviour of a perforated tube with that of a pure tube, similar tests were carried out on models of the same overall dimensions as Fig. 1, but with the outer columns replaced by continuous plates. These were cut from 3/32 in. thick sheet in order to make the cross-sectional area of the pure tube as nearly equal to that of the columns as possible (i.e. within 9 per cent

Some of the results are shown in Figs. 6, 7 and 8, Fig. 6 shows the measured and calculated rotations due to a unit torque at the free end. Figs. 7 and 8 show the bending-stress distributions and the deflection profiles for a uniformly distributed load.

4. Discussion

It has been shown that the complex three-dimensional behaviour of a framed-tube and a hull-core structure can be approximated by an equivalent plane frame technique. The sizes of the matrices involved in an analysis are thereby much

reduced, and a much larger structure may be analysed by a given size of computer.

Some experimental results have been presented from tests on small-scale model structures. It is seen in Fig. 6 that the torsional stiffness of a framed-tube can be very much less than a pure tube of the same cross-sectional area as the perimeter columns. Reasonable agreement is achieved between theory and experiment, which probably indicates that the warping of the floor slabs is of less significance than the bending coupling action. It was not possible to measure the axial stresses in the columns due to torsion, and deformations only were measured. It was found that the results obtained using the standard sectional torsional stiffness of St. Venant were much less accurate than those obtained by Vlasov's theory, which takes account of the warping of the cross-section. The latter was thus used exclusively for the inner core sections. Fig. 7 indicates how the stress-distribution in the framed-tube can be altered significantly by the addition of a core if the floor slabs are able to transmit bending actions between the two. The stresses in the columns opposite the core are subjected to additional axial stresses, which has the effect of reducing the shear lag. Similar results were obtained in the case of a channel core, although little coupling was developed on the open side of the channel [3]. The stresses in the unperforated tube are not shown, since they followed closely engineer's beam theory, with only a very small degree of shear lag being measured. At the moment it is not possible to estimate accurately the effective bending stiffness of a floor slab connecting a core and perimeter column, and the coupling effect cannot as yet be treated by the simplified technique. However, this is of little significance if in practice the floor system is not designed to transmit bending moments. Fig. 8 demonstrates how the bending stiffness of the perforated tube can be considerably less than a plain tube of the same cross-sectional area.

As well as being of interest in their own right, it is hoped that the experimental data may be useful in the assessment of the accuracy of more sophisticated methods of analysis for this type of structure.

References

1. KHAN, F.R. "Recent Structural Systems in Steel for High-Rise Buildings" B.C.S.A. Conference on Steel in Architecture, London, 1969.

2. COULL, A. and SUBEDI, N.K. "Framed-tube Structures for High-rise Buildings" Jnl. Struct. Div., A.S.C.E., Vol. 97, No. S.T.8, 1971, p.2097.

3. SUBEDI, N.K. "Hull-core Structures for High-rise Buildings", Ph.D. Thesis, University of Strathclyde, 1971.

Acknowledgement

The work described in this paper was assisted by a Grant from the Science Research Council.

Summary

A method is presented for reducing the analysis of a three-dimensional hull-core structure to that of an equivalent plane frame. Some experimental data are presented from tests on model structures subjected to bending and torsion.

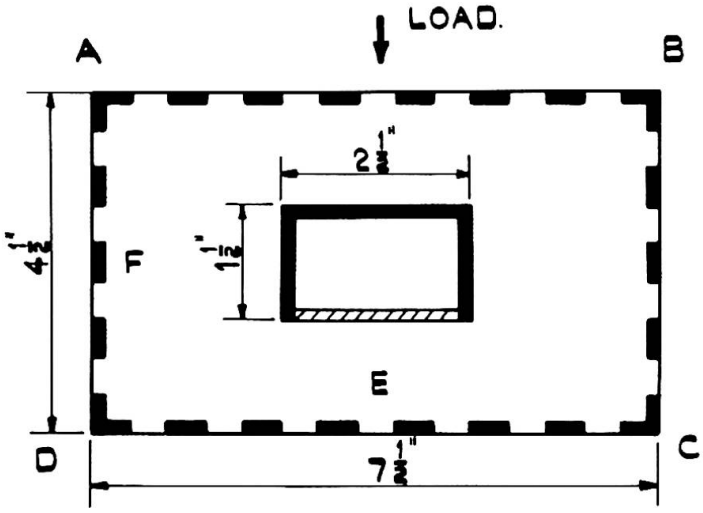

FIG. 1. HULL - CORE STRUCTURE WITH BOX OR CHANNEL CORE.

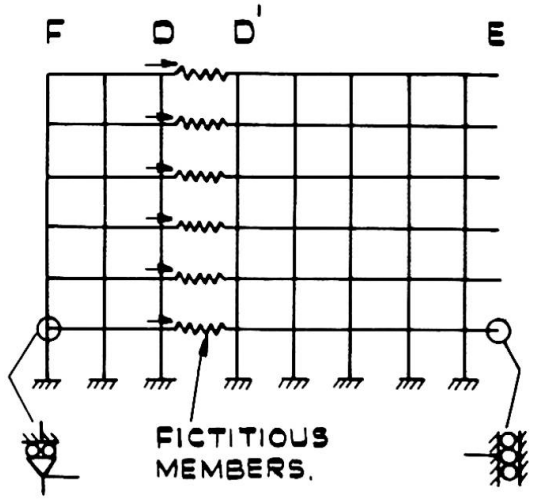

FIG. 2. EQUIVALENT PLANE FRAME.

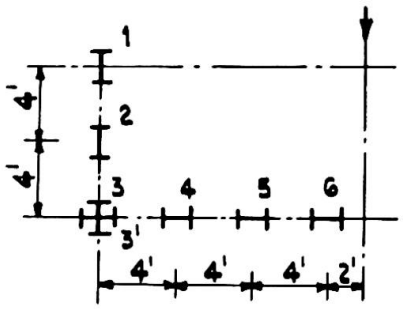

FIG. 3.

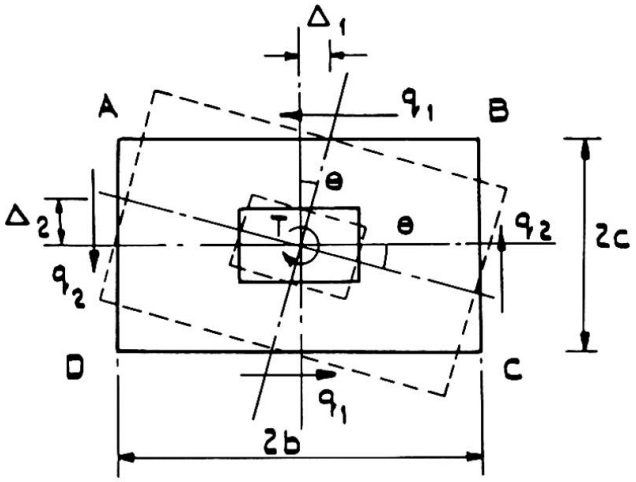

FIG. 4. ROTATION OF STRUCTURE.

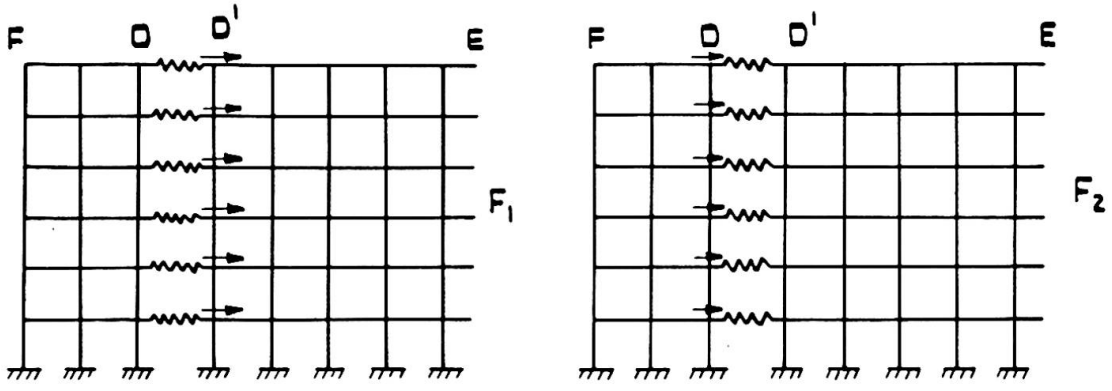

FIG. 5. DETERMINATION OF FLEXIBILITIES F_1 & F_2

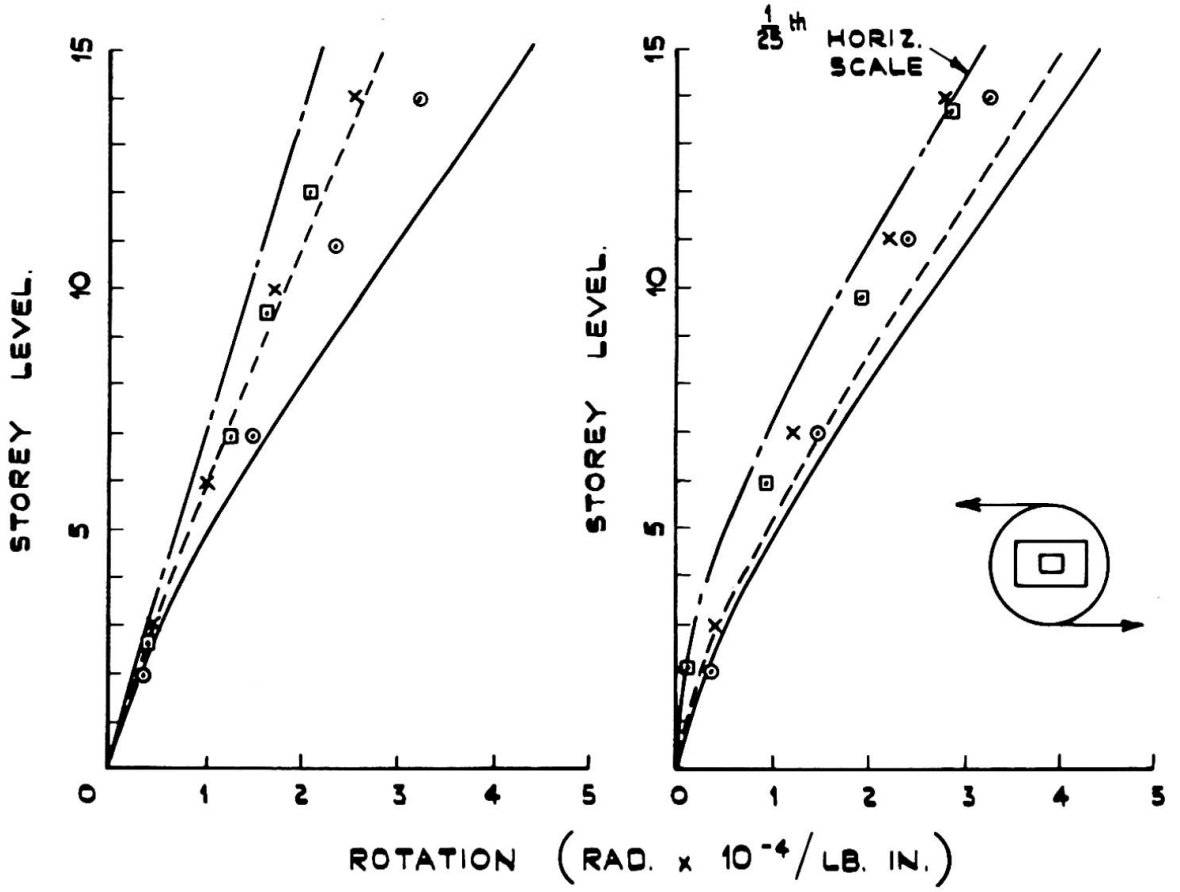

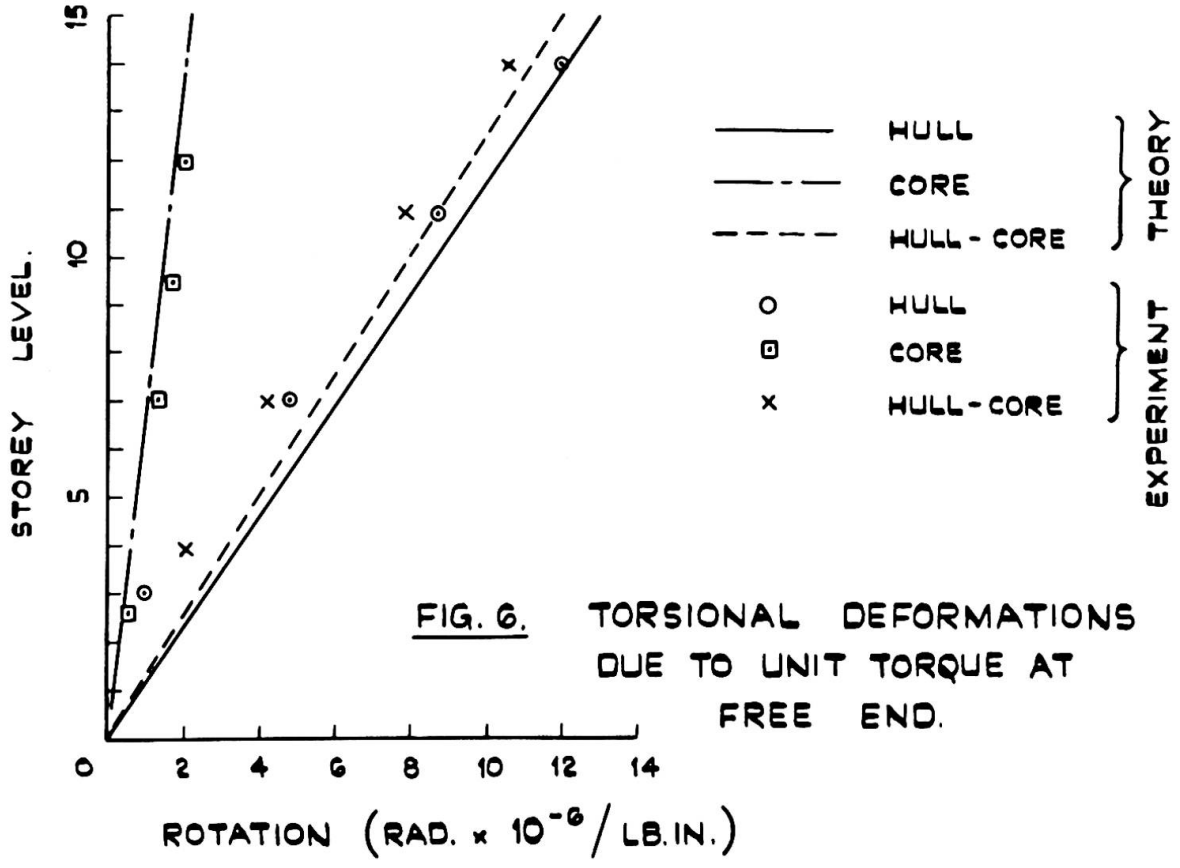

FIG. 6. TORSIONAL DEFORMATIONS DUE TO UNIT TORQUE AT FREE END.

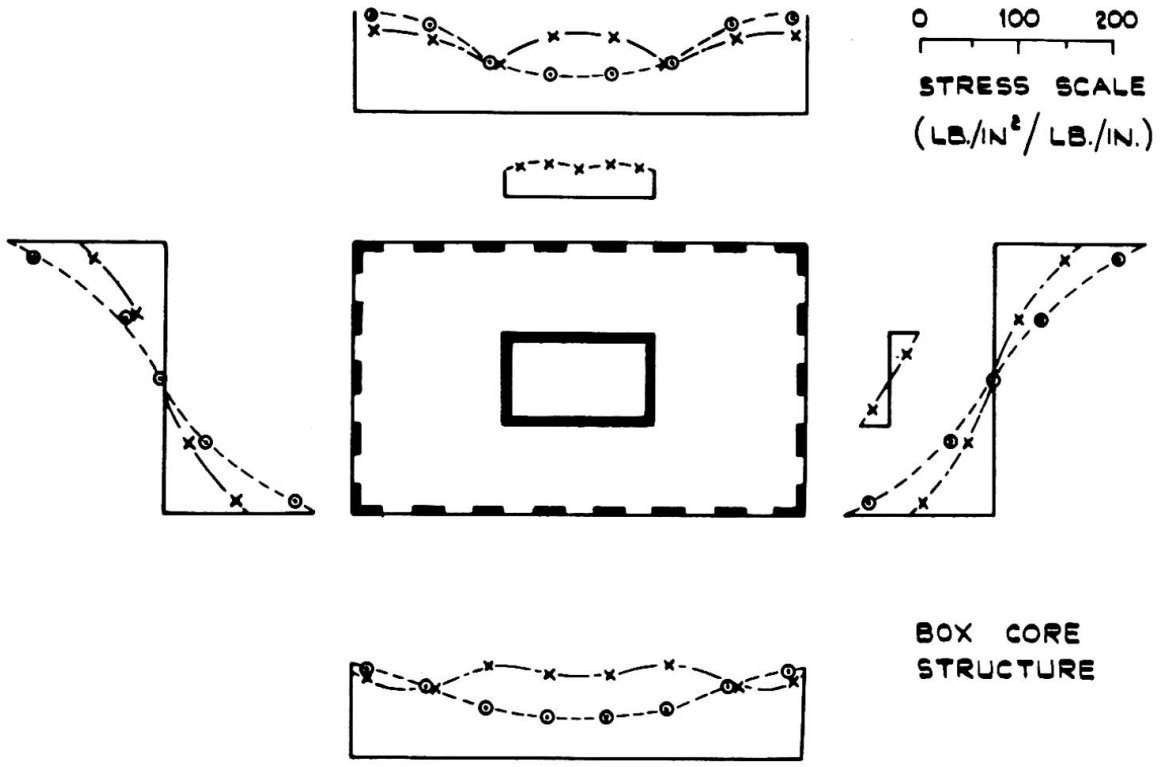

FIG. 7. STRESS DISTRIBUTION AT THIRD FLOOR LEVEL.

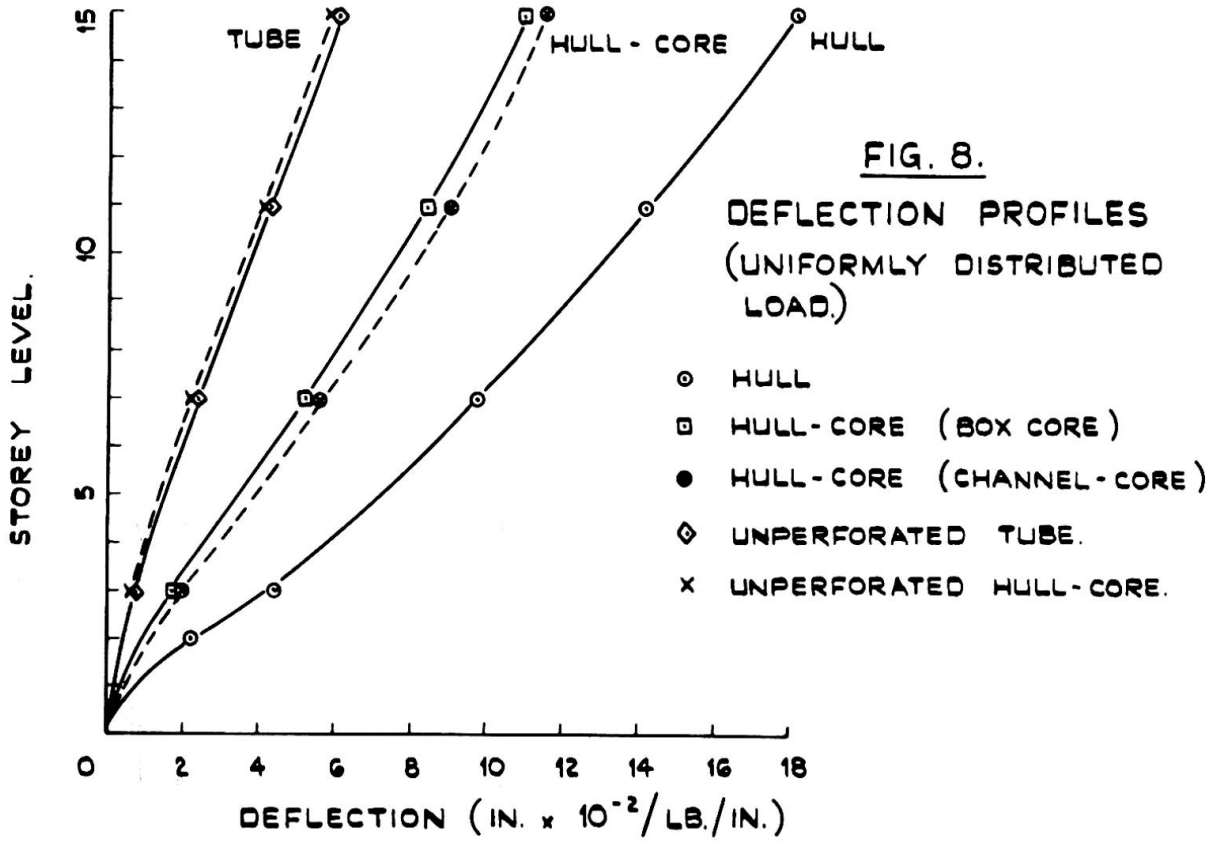

FIG. 8.
DEFLECTION PROFILES
(UNIFORMLY DISTRIBUTED LOAD.)

V

Oscillation of Cylindrical Structure in Wind

Oscillation de structures cylindriques sous l'effet du vent

Schwingungen zylindrischer Bauwerke unter Windeinfluss

NOBUHIRO UKEGUCHI HIROSHI SAKATA HIROKI TANAKA
Dr. Eng. Manager Dr. Eng. Senior Research Engineer Research Engineer

Aero-Hydraulic Research Laboratory
Mitsubishi Heavy Industries, Ltd.
Nagasaki Technical Institutes
1-1 Akunoura-machi, Nagasaki, Japan

1) Introduction

It is well-known that tall and slender structures like smokestacks, towers, etc. oscillate in wind. Many researches have been made to predict the oscillation of structures. The prediction, however, could not always be made successfully. There are many stacks in Japan for example and only a few percents of them were subjected to the oscillation.

From this fact, it can be said that the oscillation of a cylinder is easily effected by wind conditions and structural conditions. However, the effect of such conditions should be ascertained for safety and economical designs.

This paper deals with the oscillation of the cylindrical structures.

2) Review of researches conducted

Formerly, the oscillation of a circular cylinder was researched with an interest in an acoustic field known as Aeolian tone and was considered to be a forced-oscillation.

After that, a theory of random vibration was introduced and fluctuating lift forces on a cylinder were measured by Fung (1). The comparisons of experimental results based on the random vibration with the oscillations of actual stacks were made by Fujino and Nakagawa(2), Smith and McCarthy(3), and they had good agreements. In some special cases, however, the amplitude of oscillation of actual stack exceeds a result of experiment based on the random vibration.

Recently, the oscillation has been and is considered to be a self-excited or self-controlled oscillation. Lift forces on

a cylinder vary with the oscillation of cylinder and varied lift forces oscillate the cylinder, therefore the system of the oscillation is considered to have a feed back circuit.

Koopmann(4) showed that the so-called "locking in" region, in which frequencies of vortex shedding and cylinder oscillation coinside, is widened with an increase in amplitude of oscillation and vortex become less irregular. Toebes(5) ascertained fluctuating fluid flows behind a cylinder in stationary and oscillating conditions and also made sure of the correlations of flow along a cylinder axis. Bishop and Hassan(6), Ferguson and Parkinson (7) disclosed the phase difference of lift forces from cylinder oscillation. Keefe(8), Gerrard(9) showed pressures on a cylinder.

Reynolds number is an important factor in the oscillation of a structure. Roshko(10) revealed the features of aerodynamic forces at very high Reynolds number. Jones, Cincotta and Walker (11) showed the oscillating lift forces on an oscillating cylinder at high Reynolds number. Achenbach(12) made sure of the pressure distribution around a cylinder. As far as the oscillating lift force is concerned, the features of lift force are similar to that at sub-critical Reynolds number.

For a practical reason, Scruton and Rogers(13),(14) have widely investigated the oscillations of cylindrical structures and devices for suppressing the oscillation. Fiedler and Wille (15) showed flows in near wake of a cylinder standing on a surface and three-dimensionarities. Vickery(16) also ascertained three-dimensionarities and effects of shear flow which is boundary layer on a ground. Wootton(17) researched smokestack oscillations at high Reynolds number and showed a boundary of random vibration and regular vibration. Cooper and Wardlaw (18), and Vickery(19) researched on the oscillation of circular cylinder in the wake of other cylinder and revealed that the amplitude of oscillation is very large as compared with the oscillation of isolated cylinder.

According to the above mentioned researches, the oscillation of a cylinder may be a combined oscillation of self-excited and random oscillations.

3) Aerodynamic lift force on a cylinder

Lift forces have been measured by many researchers as mentioned in the previous section, and the literatures(6),(7) show lift forces on an oscillating cylinder. However, no research has been conducted to reveal how the lift forces change with each amplitude of cylinder oscillation.

The lift forces at each amplitude of oscillation have the most important role in the self-excited oscillation. Therefore, an experiment was made to get the features of lift force at each amplitde. For details of an experimental results, refer to the literature(20).

A wind tunnel was used in this experiment. The test section of wind tunnel is 1.3 meter in height and 1.0 meter in width. A cylinder of 0.15 meter in diameter and 1.0 in length was mounted on a mechanical oscillator and lift forces on the

oscillated cylinder were measured with strain gauges attached to supports. Inertia force of the model was electrically taken away by means of accelerometer.

Aerodynamic lift force has two different kinds of frequencies as shown by Toebes(5). One of which is the frequency of cylinder oscillation and the other is the frequency of Karman vortex, however, they coinside with each other in locking in region.

Absolute values of the lift forces are shown in figure 1. The lift force represents only a component having a same frequency as the mechanically oscillated cylinder has, because they were calculated through Fourier series expanding of the original lift forces.

The lift forces increase with the amplitude of an oscillated cylinder and they become maximum at Strouhal number about 0.2. The maximum points, however, move to the region of smaller Strouhal number. The locking in region was not clear, because wave forms of the lift forces were irregular, but it is considered to be between dotted lines in figure 1.

A calculation was made of standard deviations of the lift forces which mean fluctuations of lift force in each cycle, in other words, irregularities of lift force. Figure 2 shows the standard deviations. The irregularities increase with a decrease of lift force and decrease at the region where Strouhal number is near to 0.2.

Phase differences of the lift force from cylinder oscillation are shown in figure 3. There are abrupt changes in phase angles in neighbourhood of Strouhal number 0.2, and the points of abrupt changes seem to coinside with the maximum points of lift forces. The phase angles are qualitatively similar to those of literatures(6),(7), but the experiment made by Bishop and Hassan(6) showed more abrupt changes. Causes of the difference are not sure but less abrupt change might be caused by irregularities of lift forces.

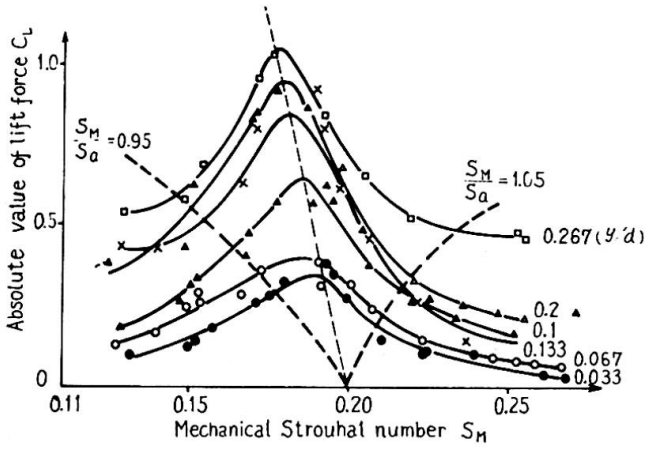

Fig.1 Absolute value of lift force

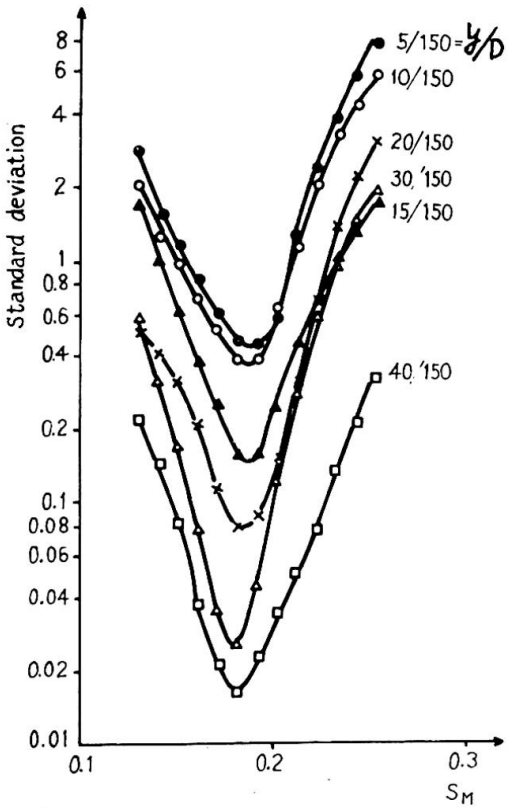

Fig.2 Standard deviation of lift force

Figure 4 shows imaginary part of lift forces which are out of phase components against the cylinder oscillation. Peak values of imaginary part versus each amplitude of the oscillated cylinder are shown in figure 5. The imaginary part does not always increase with the amplitude of oscillated cylinder, while the absolute values increase.

Lift forces obtained from free oscillation test with a cyliner on springs are also shown in figure 5. In the calculation of lift force from the oscillation test, the maximum amplitudes were used, while lift forces through the forced oscillation test were calculated as mean values. That is the reason why the result of free oscillation test showed larger forces especially at small amplitude region, and the difference might be caused by irregularities of lift forces.

4) Result of oscillation test in peculiar case

In a case of bluff cylinder, it is heard that amplitudes of oscillations versus wind velocity have hysteresis, which means that the amplitudes have different values in increasing and decreasing velocity processes. These phenomena some times occur especially in a circular cylinder with some accessories on it.

A circular cylinder with longitudinal strakes shown in figure 6 was supported on a spring system in wind tunnel. Mass of the model is 5.03 kilograms and logarithmic damping factor is 0.03. A result of the test is shown in figure 6. Solid line shows the maximum values of amplitude. When the oscillation suppressed, the amplitude does not increase

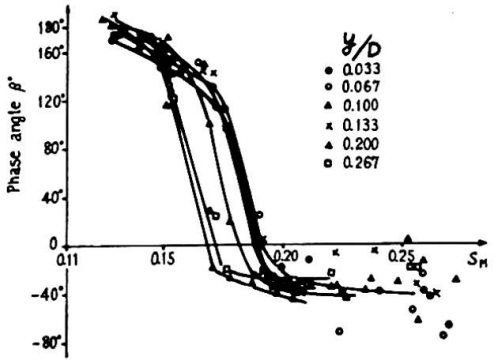

Fig.3 Phase angle

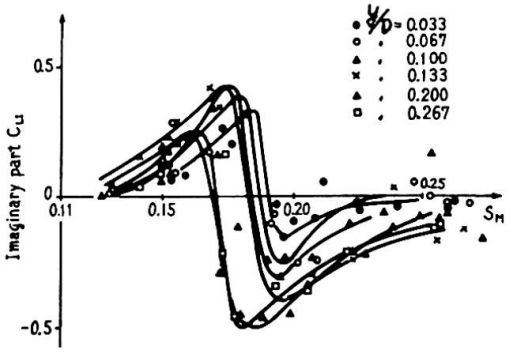

Fig.4 Imaginary part of lift

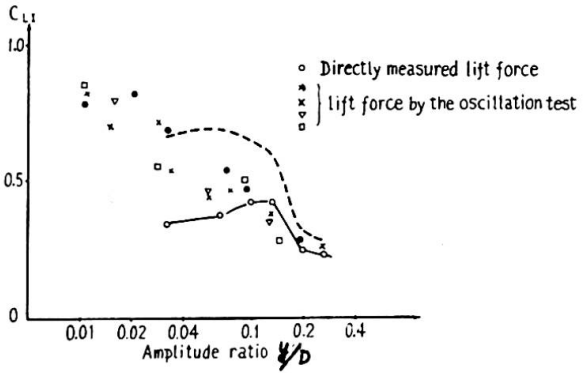

Fig.5 Peak value of imaginary part in lift force

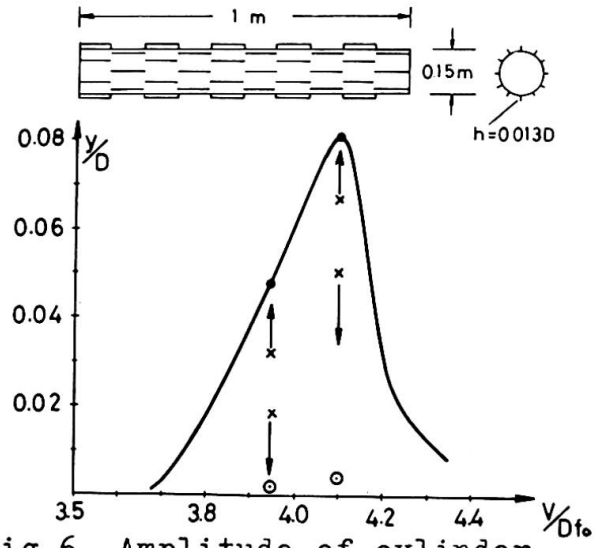

Fig.6 Amplitude of cylinder oscillation with strakes

after relieving the cylinder from the suppression. A combination of cross mark ( ) and arrow symbol indicates the amplitude increases or decreases from this initial amplitude. This shows that there are two stable points on the amplitude of oscillation.

A cylinder with trip wires of 0.06D in diameter winded around it was also tested. The model is shown in figure 7 and mass of the model is 28 kilograms and logarithmic damping factor is 0.028. A result of the test is shown in figure 7.

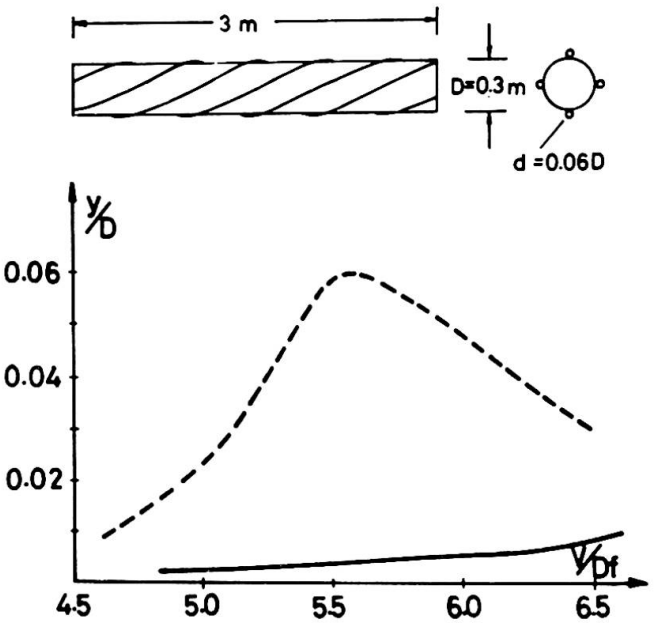

Fig.7 Amplitude of cylinder oscillation with trip wires

Solid line shows the amplitude of oscillation without any external disturbance. Once, an external disturbance acts on the cylinder, the amplitude becomes great and after that, traces the dotted line which is nearly equal to an amplitude of a cylinder with a smooth furnace. A cylinder with trip wires of 0.1D in diameter, however, did not oscillated even after a great external disturbance.

In the former case, another stability point was found by suppressing the oscillation, but in the other case, another stability point was detected by giving the external disturbance.

5) Equation of oscillation under lift forces

There are two different kinds of lift forces as mentioned in section 2) and 3). One of which is lift forces induced with a cylinder oscillation, and it causes a self-excited oscillation. The other is the so-called fluctuating lift force, and it induces a random vibration.

In a locking in region, a cylinder usually oscillates with its natural frequency, and in that case, real part of lift forces can be neglected as compared with inertia force of the cylinder.

Now, let us consider an equilibrium of cylinder oscillation as shown in figure 8. The real part and imaginary part of lift forces are oscilating with the natural frequency and so they do not move or circulate on the diagram in figure 8, however, fluctuating lift force is circulating freely.

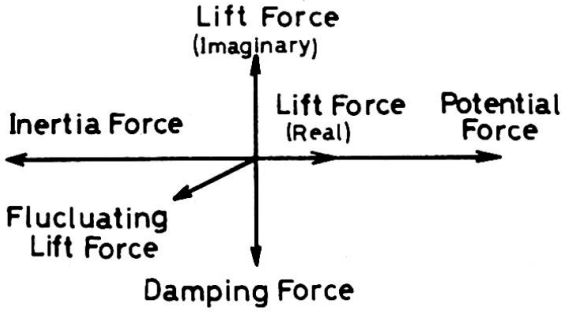

Fig.8 Diagram of cylinder oscillation

$$= -L_o y_o \omega_o \int_o^{\frac{2\pi}{\omega_o}} e^{i\omega_o t}\, e^{i\omega_o t}\, dt \int f(x) g(x)\, dx$$

$$= -\pi L_o y_o \int f(x) g(x)\, dx \qquad \text{——————} \quad (4)$$

4.4) Energy equilibrium

The oscillation of a cylinder is maintained by the above three energies, and flow of the energies per unit time must be balanced.

The energy variation is the following.

$$\frac{dT}{dt} - \frac{dW_D}{dt} + \frac{dW_a}{dt} = 0 \qquad \text{——————} \quad (5)$$

From the equations(1),(2),(4)

$$\frac{dT}{dt} = \omega_o^2 M y_o \frac{dy_o}{dt} \qquad \frac{dW_D}{dt} = W_D \frac{\omega_o}{2\pi} = -\frac{1}{2} M \omega_o^3 g y_o^2$$

$$\frac{dW_a}{dt} = W_a \frac{\omega_o}{2\pi} = -\frac{1}{2} L_o y_o \omega_o \int f(x) g(x)\, dx$$

Putting the above equations into the equation(5) the following equation can be get

$$\omega_o^2 M y_o \frac{dy_o}{dt} + \frac{1}{2}\omega_o^3 M g y_o^2 - \frac{1}{2} L_o y_o \omega_o \int f(x) g(x) = 0 \qquad \text{————} \quad (6)$$

Simplifying a little more, then

$$\frac{dy_o}{dt} + \frac{1}{2}\omega_o g y_o - A L_o = 0 \qquad \text{——————} \quad (7)$$

where $A = \frac{1}{2M\omega_o} \int f(x) g(x)\, dx$

4.5) Random vibration

If the lift force(L_o) is independent of cylinder oscillation, the equation(7) becomes a linear differential equation.

$$L = \sum L_n e^{i\omega_n t} \fallingdotseq \sum_j \frac{L_{N+j} + L_{N-j}}{2} e^{i\omega_j t}\, e^{i\omega_o t}$$

$$= \sum_j L_j e^{i\omega_j t}\, e^{i\omega_o t}$$

Then, the equation(7) becomes as follows.

$$\frac{dy_o}{dt} + \frac{1}{2}\omega_o g y_o - A \sum_j L_j e^{i\omega_j t} = 0$$

The solution is

$$y_o = -e^{-\int \frac{1}{2}\omega_o g dt} \int A \sum_j L_j e^{i\omega_j t}\, e^{\int \frac{1}{2}\omega_o g dt}\, dt$$

$$= -\sum \frac{2A L_j e^{i\omega_j t}}{g\omega_o + 2ig\omega_o} \qquad \text{——————} \quad (8)$$

The mean value is

$$\frac{1}{T}\int_o^T y_o^2\, dt = \sum \frac{2A^2 L_j^2}{(g\omega_o)^2 + (2\omega_j)^2} \qquad \text{——————} \quad (9)$$

This is the same equation as an approximate equation of random oscillation.

When the vector of fluctuating lift force directs upward, an amplitude of cylinder oscillation becomes larger and when it directs downward, the amplitude becomes smaller.

If a frequency of the fluctuating lift force is close to the natural frequency of cylinder oscillation, the vector of fluctuating lift force circulates slowly on the diagram. However, when the frequency is far from the natural frequency, the vector circulates quickly. In this case, the fluctuating lift force has no effect on the cylinder oscillation, because the inertia force is so great as compared with the lift force that the lift force can not increase the amplitude of oscillation quickly.

With the above assumption, the following equations are considered.

amplitude of oscillation $y(t) = y_0(t)e^{i\omega_0 t}$

variation of amplitude with time $\frac{dy(t)}{dt} = i\omega_0 y_0(t)e^{i\omega_0 t}$

where $\frac{dy_0(t)}{dt}e^{i\omega_0 t} \ll i\omega_0 y_0 e^{i\omega_0 t}$

An energy of oscillation is stored in the system as a kinetic energy but the damping force of a structure always discharges the energy while the lift force is supplying the energy. Unfortunately however, the energy supply is not always constant with time.

5.1) Kinetic energy

Kinetic and potential energies are exchanging each other in each cycle of oscillation and so total energy is expressed using an amplitude of oscillation.

$$T = \frac{1}{2}\omega_0^2 y_0^2 \int mf^2(x)dx = \frac{1}{2}\omega_0^2 y_0^2 M \qquad \text{(1)}$$

5.2) Scattering energy due to damping force

$$\delta W_D = D\frac{dy}{dt}dy = iM\omega_0^2 g y_0 e^{i\omega_0 t}dy$$

Scattering energy in one cycle is

$$W_D = \oint \delta W_D = iM\omega_0^2 g y_0 \int_0^{\frac{2\pi}{\omega_0}} e^{i\omega_0 t}\frac{dy}{dt}\cdot dt = -M\omega_0^3 y_0 \int_0^{\frac{2\pi}{\omega_0}} e^{i\omega_0 t}\, e^{i\omega_0 t}\, dt$$

$$= -\pi M\omega_0^2 g y_0^2 \qquad \text{(2)}$$

5.3) Energy supply due to lift force

Real part of the lift force does not supply the energy, and so only imaginary part is considered.

$$L(t) = iL_0(t)e^{i\omega_0 t}g(x) \qquad \text{(3)}$$

$$\delta W_a = L(t)dy = iL_0 e^{i\omega_0 t}dy \int f(x)g(x)dx$$

Energy supply in one cycle is

$$W_a = \oint \delta W_a = iL_0 \int_0^{\frac{2\pi}{\omega_0}} e^{i\omega_0 t}\frac{dy}{dt}dt \int f(x)g(x)dx$$

5.6) Oscillation with linear lift force

The lift force linear to the amplitude of oscillation can be expressed as follows.

$$L_0(t, y_0) = Cy_0 + \sum_j L_j e^{i\omega_j t}$$

Then, the equation(7) becomes as the following.

$$\frac{dy_0}{dt} + \left(\frac{1}{2}\omega_0 g - AC\right) y_0 - A \sum_j L_j e^{i\omega_j t} = 0 \qquad \text{(10)}$$

In this case, the oscillation changes as if the damping force of the system varied and if $2AC > \omega_0 g$, flutter occurs.

5.7) Oscillation with non-linear lift force

The lift force can be expressed as the following.

$$L_0(t, y_0) = L_0(y_0) + \sum_j F_j e^{i\omega_j t} = 0$$

The equation(7) becomes as the following.

$$\frac{dy_0}{dt} + \left\{\frac{1}{2}\omega_0 g - AL_0(y_0)\right\} - A \sum L_j e^{i\omega_j t} = 0 \qquad \text{(11)}$$

This is the equation of oscillation combined with self-excited and random ones.

6) Discussion

The lift forces on a smooth cylinder shown in figure 5 is the aerodynamic forces expressed by $L_0(y_0)$ in equation(11). The difference between lift forces through free oscillation test and forced oscillation test may be caused by the fluctuating lift forces represented by $L_j e^{i\omega t}$. Unfortunately, we did not measure the frequency components of the fluctuating lift force, but when the frequency is close to the natural frequency of cylinder oscillation, a total lift force becomes expressed by dotted line in figure 5. However, it looks like over estimated.

The lift forces $L_0(y_0)$ on a cylinder with accessories were not measured, but may be represented by solid line shown in figure 9, because there are two amplitude of oscillation. The amplitude of oscillation increases in the region where a lift force is greater than a damping force and vice versa, and so the point(1) is a stable neutral point and point(2) is unstable neutral point. If there is no fluctuating lift force, the cylinder does not oscillate at all or oscillates steadily with the amplitude of point(1). If there is a little fluctuating lift force, the lift force is added to the solid line and becomes as dotted line(1) but the added value depends on an absolute value of the fluctuating lift force and frequency component. In this case, the point (A) is a stable point and this oscil-

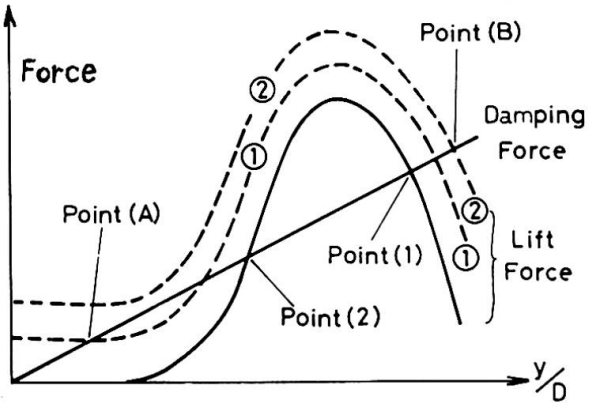

Fig.9 Oscillation mechanism of actual smokestack

lation can be considered a random vibration, because there is not any regular oscillation. If there is a great fluctuating lift force, the total lift force become like dotted line(2) and in this case, the amplitude increases till point(B) and the oscillation consists of random and regular oscillation.

Actual smokestacks or cylindrical towers have usually some accessories e.g. ladders, platforms, etc. and so the lift force against amplitude may be deformed even at very high Reynolds number. That may be the reason why, on the actual structures, some structures oscillate while the other similar structures do not oscillate.

7) Notation

D : cylinder diameter
l : cylinder length
ρ : air density
v : wind velocity
L : lift force
C_L : lift coefficient $(L/2\rho V^2 Dl)$
y : amplitude of oscillation
f_o : natural frequency
ω_o : natural angular frequency
δ : Logarithmic damping factor
S_M : mechanical Strouhal number
I : imaginary part $(f_M D/V)$
K : kinetic energy
W_D : work due to damping force
W_a : work due to lift force
$f(x)$: mode of cylinder oscillation
$g(x)$: mode of lift force
g : damping coefficient $(\delta/2\pi)$
f_M : frequency of mechanically oscillated cylinder

8) Reference

1) Y.C. Fung, Fluctuating lift and drag acting on a cylinder in a flow at supercritical Reynolds number. JAS Vol.27 No.11 1960

2) K. Nakagawa, T. Fujino, An experimental study of aerodynamic devices for reducing wind-induced oscillatory tendency of stacks. Symposium on wind effects. Paper 3, 1963

3) J.O. Smith, J.H. McCarthy, Dynamic response of tall stacks to wind excitation. ASME Paper number 63-WA-246, 1963

4) G.H. Koopmann, The vortex wakes of vibrating cylinder at low Reynolds number. J. Fluid Mech. Vol.28, Part 3, 1966

5) G.H. Toebes, The unsteady flow and wake near an oscillating cylinder. ASME Paper number 68-WA/FE-23, 1968

6) R.E.D. Bishop, A.Y. Hassan, The lift and drag forces on an oscillating cylinder. Proc. Royal Soc. of London, Series A, Vol.277, 1964

7) N. Ferguson, G.V. Parkinson, Surface and wake flow phenomena of the vortex-excited oscillation of a circular cylinder. Trans. of ASME, J. of Eng. for Industry, November 1963

8) R.T. Keefe, An investigation of the fluctuating forces acting on a stationary circular cylinder. Univ. of Toronto, Ins. of Aerophysics, Report No.76, AFOSR 2147, 1961

9) J.H. Gerrard, An experimental investigation of oscillating lift and drag of a circular cylinder shedding turbulent vortices. J. Fluid Mech. Vol.11, Part 2, 1961

10) A. Roshko, Experiments on a circular cylinder at high Reynolds number. J. Fluid Mech. Vol.10, Part 3, 1961

11) G.W. Jones, J.J. Cincotta, R.W. Walker, Aerodynamic forces on a stationary and oscillating circular cylinder at high Reynolds number. NASA TR-300

12) E. Achenbach, Distribution of local pressure and skin friction around a circular cylinder in cross-flow up to Re= J. Fluid Mech. Vol.34, Part 4, 1968

13) C. Scruton, On the wind-induced oscillation of stacks, towers and masts, Symposium on wind effects, Paper 16, 1963

14) C. Scruton, E.W. Rogers, Steady and unsteady wind loading of building and structures. Phylosophical Trans. of the Royal Soc. of London. A 269, 1971

15) H.E. Fiedler, R. Wille, Some measurements in the immediate near wake of blunt bodies. AIAA Ppaer No. 69-746, 1969

16) B.J. Vickery, Wind induced vibration of towers stacks and masts. Symposium on wind effects. Paper -2, 1971

17) L.R. Wootton, The oscillation of large circular stacks in wind. Proc. of Ins. Civil Eng. Paper No. 7188, 1969

18) K.R. Cooper, R.L. Wardlaw, Aeroelastic instabilities in wakes. Symposium on wind effects, Paper -1, 1971

19) B.J. Vickery, R.D. Watking, Flow induced vibration of cylindrical structures. 1st Australian Conf. on Hydro and Fluid Mech. 1969

20) H. Tanaka, S. Takahara, Study on unsteady aerodynamic forces acting on an oscillating cylinder. Proc. 19th Japan Cong. for Applied Mech. 1969

Summary

Tall and slender structures have a trend to oscillate in wind. The oscillation is usually in combinations of self-excited and random oscillations, and the lift force varies with the amplitude of cylinder oscillation. The lift force on a cylinder with accessories is so deformed that, some times, a trigger is needed to oscillate the cylinder. Fluctuating lift force due to turbulence in natural wind or in wake of other structures may become the trigger.

V

Experimental Verification of the Dynamic Characteristics of a Free-Standing Tower

Vérification expérimentale des caractéristiques dynamiques d'une tour isolée

Experimentelle Nachprüfung der dynamischen Eigenschaften eines freistehenden Turmes

ARTHUR N.L. CHIU
Professor of Engineering

GEORGE T. TAOKA
Associate Professor of Civil Engineering

University of Hawaii, USA

1. INTRODUCTION

A free-standing, three-legged, latticed steel tower has been instrumented for studying its dynamic response to wind forces. This paper describes the location of the structure, the structural details, the mathematical representation of the structure, and the computed and experimentally determined dynamic characteristics of the tower. The tower is 150 feet high, and is located at the U.S. Marine Corps Air Station, Kaneohe Bay, on the island of Oahu, Hawaii. Permission for its use in this investigation was granted through the courtesy of the Station because this tower is part of a transmitting system that will be replaced and the tower is no longer needed in the present communication system.

A mathematical model of the tower was formulated from structural detail drawings of the structure. The first three translational frequencies and mode shapes were calculated for two orthogonal horizontal directions. The tower was then subjected to man-excited oscillations, and the fundamental frequency and critical damping ratio for the first mode were determined, for the same directions, from accelerograms. Finally, a Fourier Analysis was performed on the accelerograms for the tower under ambient conditions, and the first two periods were obtained for both directions. There was good agreement among the predicted and experimentally determined natural frequencies.

2. DESCRIPTION OF THE TOWER

Figure 1 shows the tower as seen from the north. The horizontal coordinate directions in Table 1 show that the x direction points to the west and the y direction to the south. Each leg of the tower is rigidly attached to a concrete footing at the base. The three concrete footings extend approximately 10 feet below the ground and are approximately 11 feet square at the bottom. Details concerning wind conditions at the tower site are given in Ref. [1].

The tower is fabricated from steel angles and is triangular in cross-section with 14 panel points. It is 25 feet wide at the base and tapers at a constant slope from the base to the third panel point which is 143 feet above the base. From the third panel point to the top, the tower width is constant at 4 feet. Riveted connections are used throughout the structure. All connections and structural members are relatively rust-free because all components were galvanized prior to construction. Figure 2 shows the structural details of the individual members of the structure.

Table 1 lists the projected areas and masses that were assumed to be concentrated at panel points for the mathematical model. Additional steel plates were welded on the horizontal struts at the two levels of the existing platforms to minimize the effect of torsional movements that could be induced because of eccentric mass distributions caused by the platforms.

3. INSTRUMENTATION

Open grating platforms were constructed in the center of the tower for placing accelerometers and anemometers at the five levels shown in Figure 2. A total of 10 Systron-Donner, Model 420, force balance type accelerometers were placed at each of the five levels of the tower as shown in Figure 3. Two accelerometers were mounted in each casing parallel to the x and y axes shown in Figure 2. Two R.M. Young, Model 27101X, Gill Anemometers were also placed at each of the five levels to measure the x and y components of the wind velocity as shown in Figure 4.

Analog signals from these accelerometers and anemometers were relayed via shielded cables to a Multiplexer-Analog/Digital Converter Unit (Redcor Corp., Model 720), and the resulting digital information was recorded on a 9-track, 800 BPI, magnetic tape by a Magnetic Tape Recorder (Cipher Data Products Model 70H). The Multiplexer-Analog/Digital Converter and Magnetic Tape Recorder System is housed in a building approximately 200 feet from the tower, and the front panel of the system is shown in Figure 5.

4. MATHEMATICAL MODEL AND COMPUTED RESULTS

The tower was idealized as a space truss, and the structural members were assumed to resist axial loads only. Horizontal loads were assumed to be applied only at panel points, and secondary stresses were assumed to be negligible. Under these assumptions, the column elements of the flexibility matrix were computed by successively applying a unit load horizontally at each panel point in the x or y direction.

For the dynamic analysis, the tower was modeled mathematically as a discrete system of fourteen masses lumped at the panel points as listed in Table 1. The mass between midheights above and below a panel point was concentrated at that point and assumed to be located at the centroid of the horizontal cross section. The mass may move in the horizontal plane designated by the x and y axes of Figure 2, but vertical motions were considered negligible. Motions in the horizontal directions were assumed to be uncoupled. The mass matrix was diagonal and identical for motion in both x and y directions. The base of the tower was assumed to be rigid; therefore, the entire tower was assumed to behave as a lumped mass cantilever beam.

The first three translational natural periods and corresponding mode shapes in each direction for this tower were computed on the IBM 360, Model 65, digital computer at the University of Hawaii. These periods were 0.537 sec, 0.169 sec, and 0.084 sec in the x direction, and 0.496 sec, 0.158 sec, and 0.080 sec in the y direction. The corresponding mode shapes are given in Table 2.

5. EXPERIMENTAL RESULTS

The tower was subjected to man-excited oscillation in the x and y directions according to the method discussed by Hudson, *et. al.* [2], to obtain natural periods of vibration of the tower. This experiment was repeated several times on different days of fairly calm wind conditions, so that damping effects could also be estimated, and the results were averaged. Figure 6 shows portions of accelerograms obtained at the top instrumentation

level (150 ft) for motions in the x and y directions. These records substantiate the assumption that vibration in the two orthogonal horizontal directions are uncoupled. Vertical and horizontal motions of the supports were not discernable from response records taken at the bases and hence the assumption of a rigid foundation is valid.

It was fairly easy to force the tower into vibrating in a purely fundamental mode as shown in Figure 6. From records such as these, the fundamental periods of vibration were determined for the two directions. It was difficult to force the tower into vibrating purely in the second or third modes. Figure 7 shows the responses caused by wind. The fundamental mode predominates although the second and third modes are discernable occasionally at relatively much smaller amplitudes of vibration. Thus, close inspection of the chart records for small ambient amplitudes of vibration permits estimates of these higher modes.

Table 3 shows good agreement among the predicted and experimentally determined natural periods of vibration for the first three translational modes. The periods determined from field data were 0.54 sec, 0.18 sec, and 0.08 sec for the x direction, and 0.50 sec, 0.16 sec, and 0.09 sec for the y direction.

Table 4 compares the experimental and predicted first mode shape. The experimental points were determined by taking ratios of the simultaneous amplitude of the accelerogram records for the various levels. All mode shapes are normalized with respect to the top level.

Critical damping ratios for the fundamental modes of vibration from the man-excited records were estimated using the logarithmic decrement method that is applicable when damping is small. Damping for the fundamental mode was estimated from several sections of the field data. The averaged critical damping ratios were approximately 0.3 and 0.5 percent of critical in the x and y directions, respectively.

A ladder which was attached to the leg of the tower along the y direction probably contributed to the difference in natural periods and critical damping ratios between the two horizontal directions. This ladder probably slightly increased the stiffness and energy absorption capacity along the y direction.

6. FOURIER ANALYSIS OF AMBIENT VIBRATION RECORDS

Digitized accelerograms on magnetic tape were subjected to Fourier analysis to determine the natural periods of vibration of the tower. Each continuous accelerogram consisted of 1023 data points taken at intervals of 0.025 seconds, for a time length of approximately 25.55 seconds. The resulting Nyquist frequency of 20 Hz is thus well above the first three frequencies of the tower in either direction. Similar studies have been reported recently by Murota and Ishizaki for a tower [3], and by Van Koten [4], and Trifunac [5] for buildings.

Although the natural periods could be obtained from the analysis of only one record in each direction, the frequency resolution of approximately 0.04 Hz was not considered satisfactory for this analysis. Thus longer records consisting of four sequential records connected together were used for both x and y horizontal directions. Because two data points between each individual record were lost due to a time gap between each record, these values were assumed to be equal to the mean for this analysis. While this procedure may introduce slight errors [6], its effect on the estimate of the lower frequencies in the Fourier Amplitudes was considered small enough to yield satisfactory values in this range.

The total time of each lengthened record corresponded approximately to 100 seconds, thus giving a frequency resolution of 0.01 Hz. Such lengthened accelerograms for the accelerometers at the top of the tower were subjected to computer analysis. A Fast Fourier Transform Program developed by Sande [7] was used to obtain the Fourier coefficients of the accelerograms. The coefficients were then modified by the formula: $(F_i)_M = 0.25\ F_{i-1} + 0.50\ F_i + 0.25\ F_{i+1}$, where $(F_i)_M$ and F_i are respectively the modified and original coefficients of point i. Figure 8 shows the squared modified Fourier coefficients plotted as a function of frequency.

From this figure, the two lowest translational frequencies in the x direction are 1.88 and 5.48 Hz, corresponding to natural periods of 0.53 and 0.18 seconds. For the y direction they are 2.03 and 5.85 Hz, or natural periods of 0.49 and 0.17 seconds. These are in agreement with values determined by other methods described previously (Table 3). The third translational frequencies were barely discernable in Figure 8; a torsional frequency of 7.39 Hz is also evident.

7. CONCLUDING REMARKS

The mathematical model of the tower, with the flexibility coefficients derived by assuming an idealized space truss and with lumped masses at the panel point, is adequate. Experimental data substantiated the assumptions of a rigid foundation and of essentially uncoupled motions in the horizontal orthogonal directions. Previous studies showed that three translational modes are adequate for dynamic analysis of free-standing towers that do not have eccentric distributions of masses.

The experimental data showed that the fundamental mode of vibration predominates in free-standing structures such as the tower used for this study. There was good agreement among the predicted and experimentally determined natural translational periods. Results from the Fourier analysis of ambient vibration records corroborated these periods. The tower has a fairly low damping ratio for the fundamental mode of vibration.

8. ACKNOWLEDGMENTS

The support from the National Science Foundation (Grant NSF-GK-13076) for the total research project, of which this is a part, is gratefully acknowledged. The cooperation of the U.S. Marine Corps Air Station, Kaneohe Bay in this project is appreciated very much. Acknowledgment is also made of the able assistance of Paul Santo and Mark Shimabukuro, Guy Rothwell, Jr., the Statistical and Computing Center, and the Center for Engineering Research of the University of Hawaii.

9. BIBLIOGRAPHY

1. Chiu, A. N. L., and G. T. Taoka, "Dynamic Characteristics of a Free-Standing Latticed Steel Tower," Technical Bulletin No. CE 71-B5, Department of Civil Engineering, University of Hawaii, November 1971.

2. Hudson, D. E., W. O. Keightley, and N. N. Nielsen, "A New Method for the Measurement of the Natural Period of Buildings," Bulletin of the Seismological Society of America, February 1964.

3. Murota, T., and Ishizaki, H., "Deformations and Vibrations of Some Actual Structures Due to Wind," presented at the Third International Conference on Wind Effects on Buildings and Structures, Tokyo, September 1971.

4. Van Koten, H., "The Comparison of Measured and Calculated Amplitudes of Some Buildings and Determination of the Damping Effects of the Buildings," presented at the Third International Conference on Wind Effects on Buildings and Structures, Tokyo, September 1971.

5. Trifunac, M. D., "Ambient Vibration Test of a Thirty-nine Story Steel Frame Building," EERL 70-02, California Institute of Technology, July 1970.

6. Jones, R. H., "Spectrum Estimation with Missing Observations," to appear in Annals of the Institute of Statistical Mathematics, Tokyo.

7. Gentlemen, W. M., and Sande, G., "Fast Fourier Transforms, for Fun and Profit," Proceedings of Joint Fall Computing Conference, AFIPS, Vol. 29, San Francisco, November 1966.

SUMMARY

The dynamic characteristics of a free-standing latticed tower, obtained from analysis and field experiment, are discussed. Results from a Fourier analysis of ambient response records are also presented. There was good agreement among the three sets of answers for the translational frequencies.

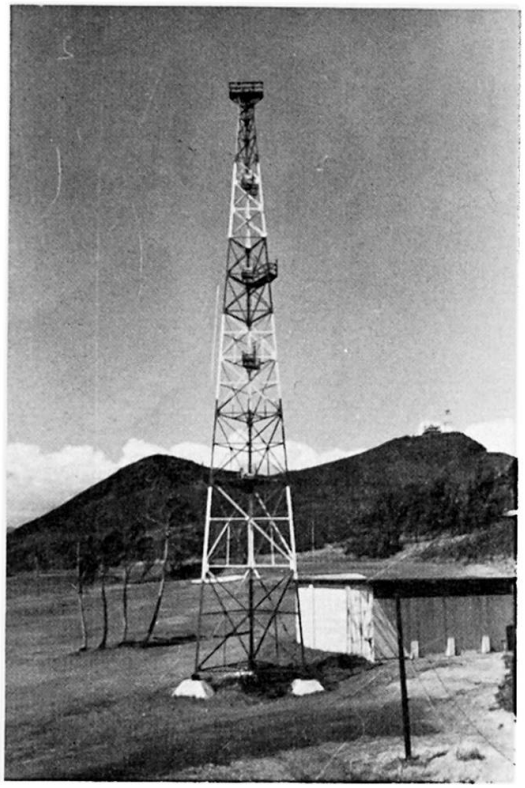

FIG. 1 – NORTH VIEW OF TOWER

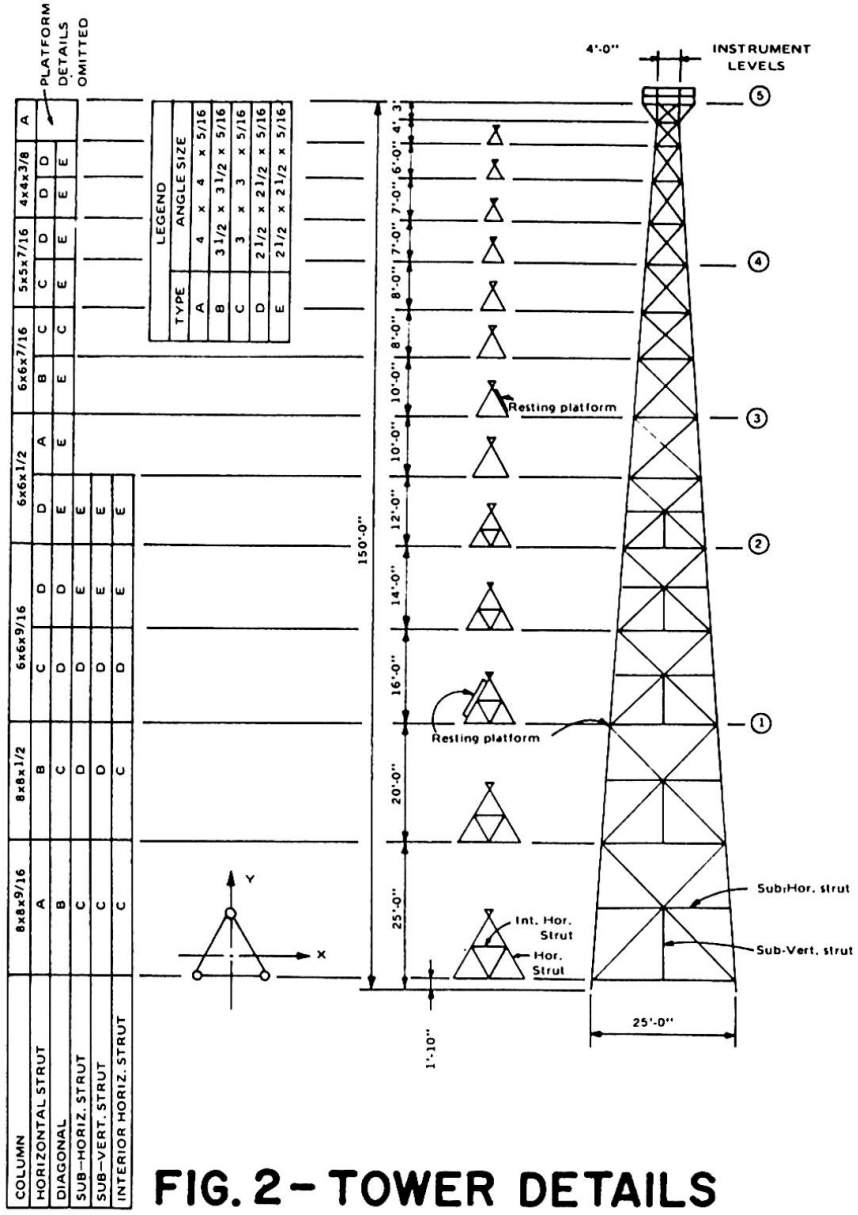

FIG. 2 – TOWER DETAILS

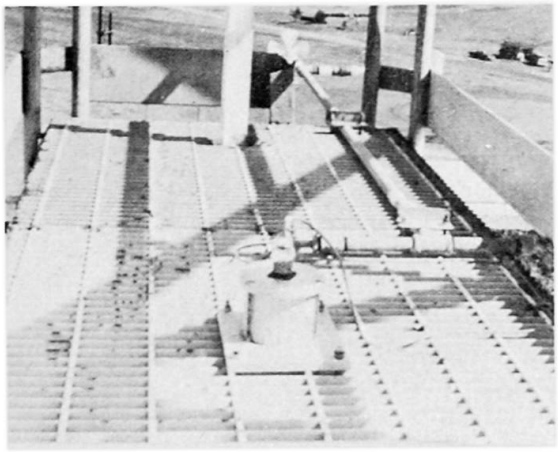

FIG. 3 – LOCATION OF ACCELEROMETER

FIG. 4 – ANEMOMETER IN PLACE

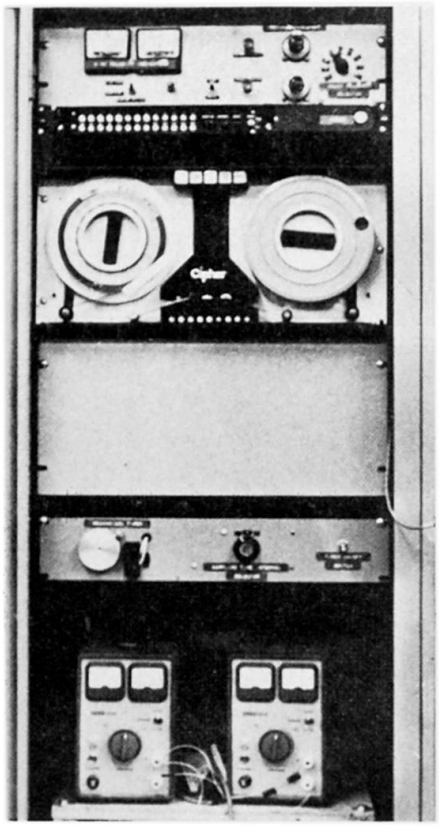

FIG. 5 – FRONT VIEW OF INSTRUMENT PANEL

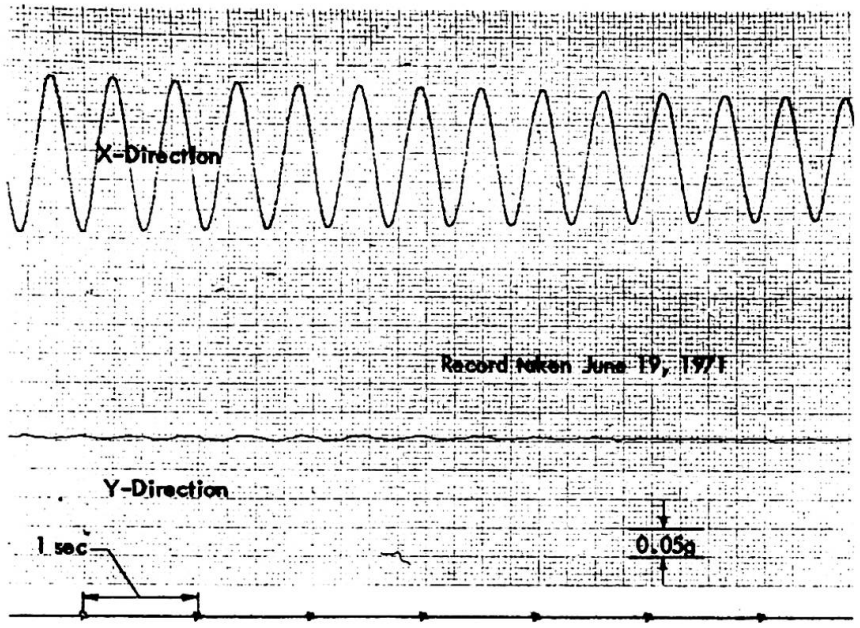

Force Applied in the X-Direction

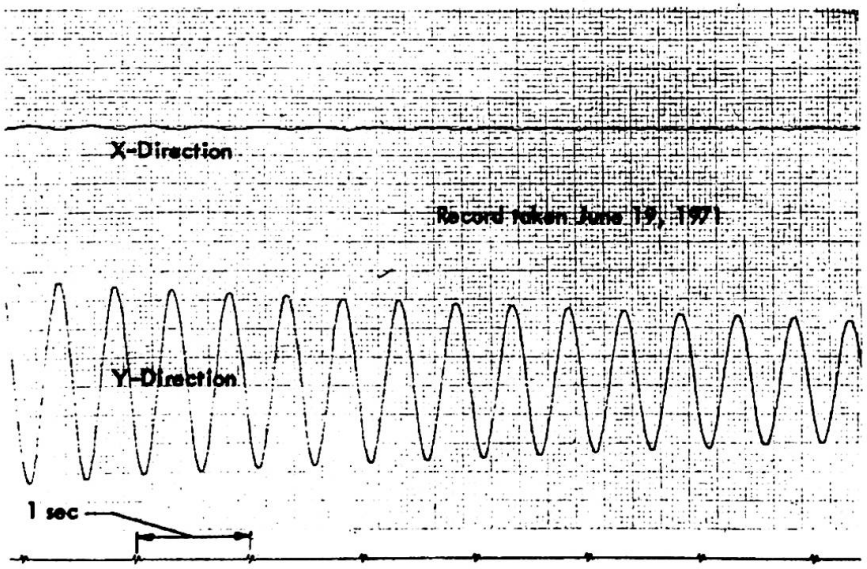

Force Applied in the Y-Direction

FIG. 6 – MAN-EXCITED RESPONSE RECORDS

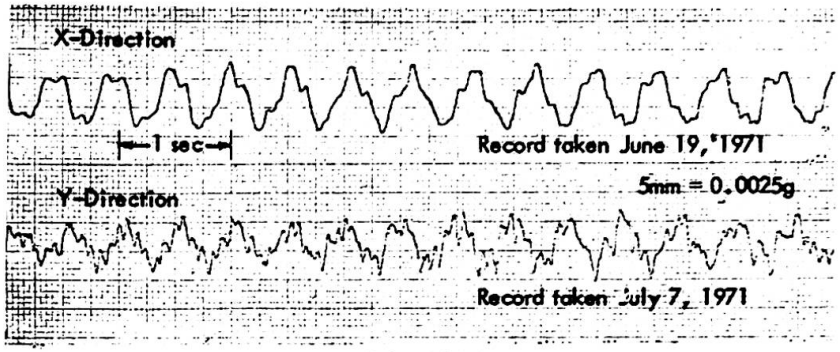

FIRST MODE

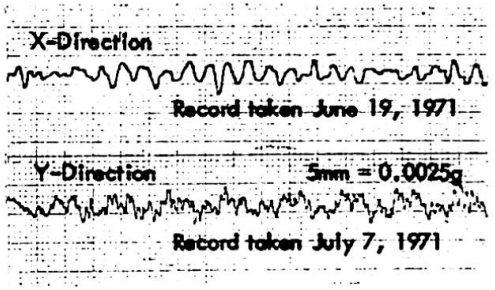

SECOND MODE

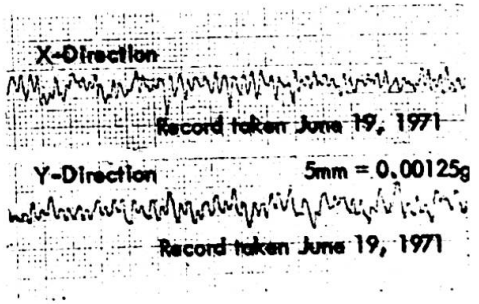

THIRD MODE

FIG. 7 – AMBIENT RESPONSE RECORDS

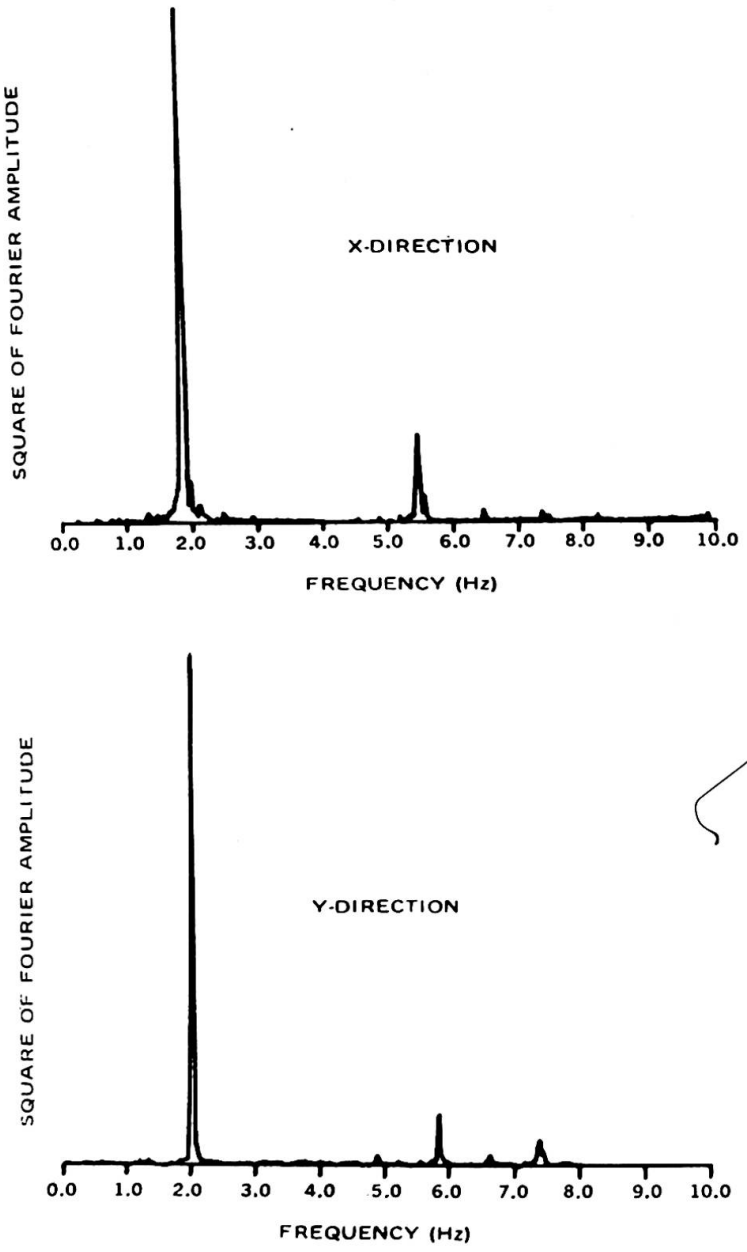

FIG. 8 – FOURIER AMPLITUDE SPECTRA

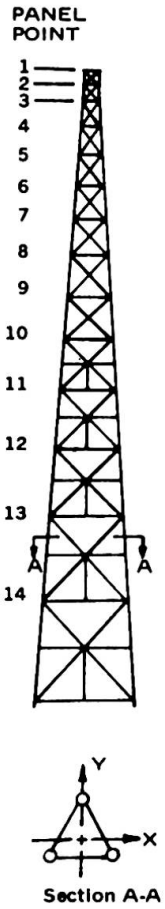

TABLE 1

CONCENTRATED MASSES AND PROJECTED AREAS

Panel Point	Elev. (ft)	Projected Area (sq.ft.)	D.L. (LB.) at Panel Point
1	150	2.87	1810
2	147	5.22	510
3	143	8.06	750
4	137	8.75	810
5	130	10.32	920
6	123	11.97	1790
7	115	14.12	1190
8	107	16.76	1360
9	97	19.30	2940
10	87	23.32	1900
11	75	28.08	3580
12	61	32.35	2940
13	45	43.45	5670
14	25	60.37	5240

NOTE: 1. Values for projected area are for one face only.

2. Values for D.L. are for entire tower.

TABLE 2

COMPUTED NORMALIZED MODE SHAPES
(Normalized with respect to bottom panel)

Panel Point	X DIRECTION First Mode	X DIRECTION Second Mode	X DIRECTION Third Mode	Y DIRECTION First Mode	Y DIRECTION Second Mode	Y DIRECTION Third Mode
1	44.05	-6.16	1.93	39.93	-5.60	1.78
2	42.19	-5.15	1.30	38.31	-4.73	1.23
3	39.69	-3.77	0.42	36.15	-3.59	0.52
4	36.11	-1.98	-0.56	33.00	-2.00	-0.41
5	32.15	-0.20	-1.41	29.50	-0.38	-1.14
6	28.46	1.25	-1.79	26.22	0.93	-1.56
7	24.55	2.49	-1.76	22.71	2.10	-1.63
8	20.98	3.35	-1.43	19.47	2.95	-1.44
9	16.94	3.99	-0.87	15.82	3.61	-0.90
10	13.39	4.14	-0.06	12.56	3.83	-0.21
11	9.71	3.94	0.80	9.18	3.72	0.63
12	6.25	3.26	1.46	5.96	3.13	1.29
13	3.32	2.23	1.66	3.19	2.20	1.56
14	1.00	1.00	1.00	1.00	1.00	1.00

TABLE 3

COMPUTED AND EXPERIMENTALLY DETERMINED NATURAL PERIODS OF VIBRATION

	Period (Sec.)					
	X DIRECTION			Y DIRECTION		
Mode	Computed	Experimental (a)	Experimental (b)	Computed	Experimental (a)	Experimental (b)
1	0.537	0.54	0.53	0.496	0.50	0.49
2	0.169	0.18	0.18	0.158	0.16	0.17
3	0.084	0.08	--	0.080	0.09	--

a - Chart records; b - Fourier Analysis

TABLE 4

COMPARISON OF COMPUTED AND EXPERIMENTALLY DETERMINED FIRST MODE SHAPE

Instrument Level	Elevation (Ft.)	X DIRECTION Computed	X DIRECTION Experimental[a]	Y DIRECTION Computed	Y DIRECTION Experimental[a]
5	150	1.000	1.00	1.000	1.00
4	123	0.646	0.67	0.656	0.71
3	97	0.385	0.40	0.396	0.45
2	75	0.220	0.25	0.230	0.28
1	45	0.075	0.10	0.080	0.11

a - Chart records

V

Scale Model Tests of a 170-meter High Sculptural Tower

Essais sur modèle réduit d'une tour de 170 m de hauteur

Versuche am massstäblichen Modell eines Turmbauwerkes von 170 m Höhe

HAJIME UMEMURA
Professor at the University of Tokyo, Eng.D., Japan

HIDEYUKI TADA
Associate Director, Nikken Sekkei Ltd, Eng.D., Japan

YASUHISA SONOBE
Professor at Chiba Institute of Technology, Eng.D., Japan

1. Introduction

The 170 m high PL Peace Tower, shown in Figs. 1 and 2, was constructed in Osaka, Japan in 1970. The tower is composed of a rigid reinforced concrete foundation which supports a 12 m high steel framed reinforced concrete podium of rigid construction which in turn supports a tubular steel tower structure. The tower portion is covered with a shotcreted crust which makes the tower into a huge sculpture of highly complicated configuration. In order to obtain basic data for earthquake and wind resistant design of this tower of unprecedented shape, extensive research studies comprising observation of micro tremors of the ground; wind tunnel tests using 1/100 scale models; static loading tests on 1/33 models including those tested to failure; free vibration tests; bending and shearing tests on shotcreted crust of the tower models, etc. were conducted. In addition, the actual vibration of the tower was observed upon its completion.

Fig. 1 PL Peace Tower

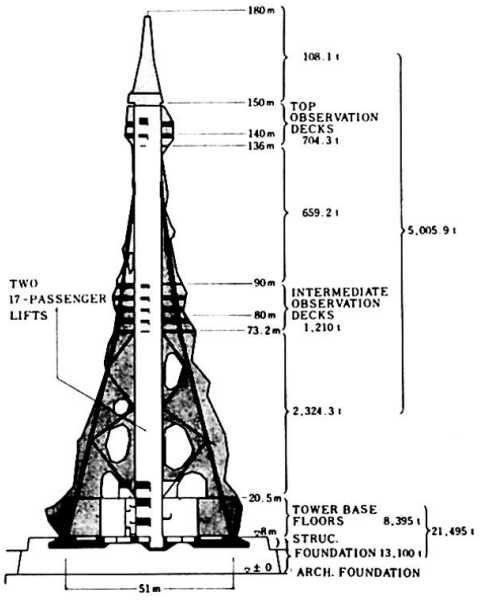

Fig.2 Illustrative Drawing

This report deals with the experimental test on 1/33 scale models conducted for the purpose of obtaining some basic data on which to base a simulated vibration model for a dynamic structural analysis. The experiments consisted of the load-by-gravity tests, the concentrated lateral load tests and the free vibration tests at various loading stages. While the load-by-gravity tests were non-rupture tests in which the lateral forces proportional to the weights of various parts of the tower were applied, the concentrated lateral loading tests were carried to the failure of the specimens.

2. Test Models

Based on the original design height of the tower which was 160 m, the scale of 1/33 was adopted for the models, taking into account the available space of the testing station. This scale resulted in the models having a height of 4.697 m, with all other dimensions similarly reduced, the original form of the proposed tower being maintained. The models were framed by the use of the same materials as those used for the actual tower, i.e., [] - 150 x 75 x 20 x 4.5 for the central shaft and steel bars for inclined columns, diagonal webs and upper framework of the tower. Two models, A and B, were prepared, both provided with horizontal diaphragms so as to facilitate the preparation of the tower shaft which was of a very complicated form. The models were designed to have sectional area of steel five times as large as that proportional to a 1/33 scale model.

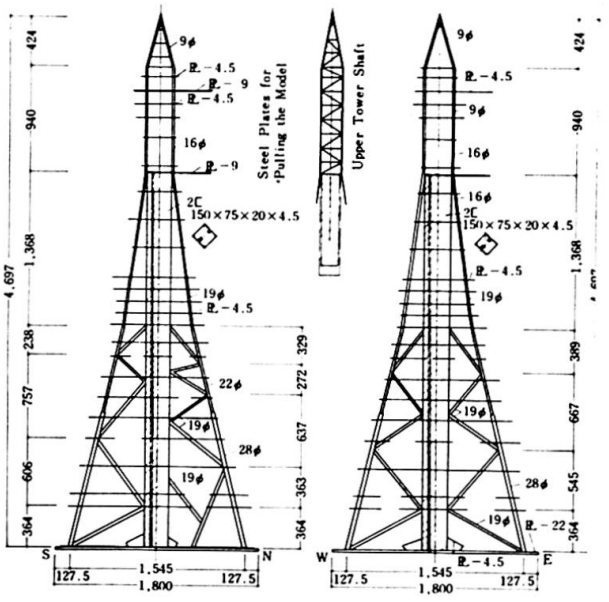

Fig. 3 Framing of the Model

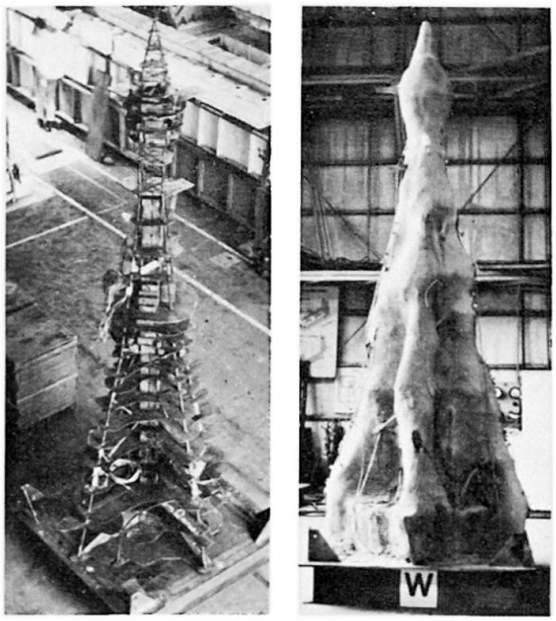

Fig. 4 Model

The outer crusts of these models were composed of shotcrete on wire laths placed on the outer face of diaphragms, all applied in the same manner as proposed for the actual tower.

The models were somewhat simplified when compared with the actual tower which, with self-standing columns and branch-like members, is very complicated; however, the basic characteristics of the tower configuration is considered fairly well represented by the models. The cross sectional area of the shotcrete crust turned out to be 11 times and 14.5 times as large as that proportional to 1/33 models with regard to Model A and Model B respectively.
In the load-by-gravity tests where the test loads were casued by the models' own weight, slabs of steel were attached to the upper and intermediate observation deck levels so as to cause the gravity loads corresponding to the loads to which these decks would be subjected to.

Tables 1 and 2 show the measured data of the completed models. Mechanical properties of shotcreted crust and structural steel are shown in Tables 3 and 4. The load-by-gravity tests and concentrated load tests were conducted when the shotcrete was aged one week and five weeks respectively.

Table 1. Weight of Models

	Model A	Model B
	(kg)	(kg)
Steel frame, Diaphragm	690	690
Added weight	500	500
Total steel weight	1 190	1 190
Shotcrete (ρ = specific gravity)	570 (ρ = 2.01)	570 (ρ = 2.14)
Total weight	1 760	1 990
Mean thickness of shotcrete	2.18 cm	2.89 cm

Table 3. Mechanical Properties of Steel

Steel	Sectional area	Yield point	Tensile strength	Elongation ratio
	(cm^2)	(t/cm^2)	(t/cm^2)	(%)
28 ø	6.256	2.86	4.47	32
22 ø	3.841	3.04	4.98	30
19 ø	2.821	3.07	4.93	31
16 ø	2.019	2.96	4.56	33
9 ø	0.593	2.86	4.29	33
℄- 4.5 ([]- 150 x 75 x 20 x 4.5)	-	2.73	4.04	32

Table 2. Relationship of Cross Section and Weight of Actual Structure to Those of Models

		Values by measurement on models	Values as designed for models
Model A	Sectional area of steel	$(\ )^2 \times 5$	$(\ )^2 \times 5$
	Sectional area of shotcrete	$(\ )^2 \times 11$	$(\ )^2 \times 5$
	Total weight	$(\ )^3 \times 17.6$	$(\ )^3 \times 10$
Model B	Sectional area of steel	$(\ )^2 \times 5$	$(\ )^2 \times 5$
	Sectional area of shotcrete	$(\ )^2 \times 14.5$	$(\ )^2 \times 5$
	Total weight	$(\ )^3 \times 20$	$(\ )^3 \times 10$

( ) = Value proportional to 1/33 scale model

Table 4. Mechanical Properties of Shotcrete

	Material age	Compressive strength (kg/cm^2)	Crushing strength (kg/cm^2)	Young's Modulus ($\times 10^5$ kg/cm^2)
Model A	1 week	298	28.7	1.97
	5 weeks	386	-	1.82
Model B	1 week	174	16.0	1.43
	5 weeks	165	-	1.20

3. Methods of Testing

Of the two loading methods, the loading-by-gravity was planned so that the lateral loads proportional to various members would be imposed on the members. For this purpose, the models were fixed at the base and were turned up and down. This type of loading may be considered to have simulated the conditions caused by the vibration of the fundamental mode. The intensity of the loading was rather small compared with the strength of materials used for the models; therefore, the experiments were conducted only within the elastic range of the models. On the contrary, the concentrated loading was intended to simulate the conditions under the ultimate loading.

In the load-by-gravity tests, each model constructed in an upright position was placed on a rotating hub of the testing apparatus together with the tower-shaped gauge holders which surrounded the model and the model was turned up and down 180° as shown in Figs. 5 and 6. In turning round the model the angle of rotation was controlled by means of a chain block and a pulley. The rotation was in north-south direction. The deflections of the models were measured with dial gauges whereas their strain were measured with wire strain gauges. The behaviours of steel under loading were observed by means of high-sensitive semi-conductor gauges which were used in combination with the aforesaid gauges. In addition, a total of nine measurement instruments as shown in Fig.7, four on compressive side and five on tensile side, were mounted along the outermost faces of each model in order to measure the local curvature variation of the outer crust.

For the concentrated loading tests, the model was connected to the loading wall by the use of a cable, which was pulled by means of a chain block so that a tensile force was imposed on the model. The cable was so supported as to be in a horizontal position during the test. For each model, the deflection was measured at Point 1 (apex), Point 2 (4.048 m in height) and Point 3 (3.333 m in height), and the load was imposed at Points 2 and 3. Deflections and strains were measured by the use of same instruments as those used for the load-by-gravity tests.

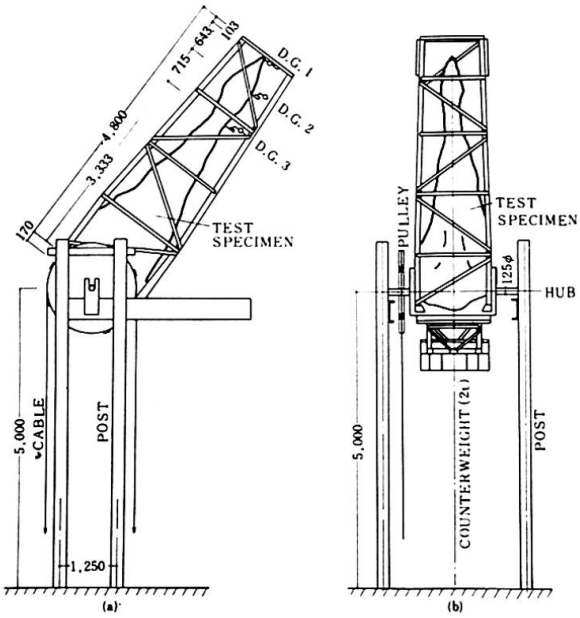

Fig. 5 Loading Apparatus

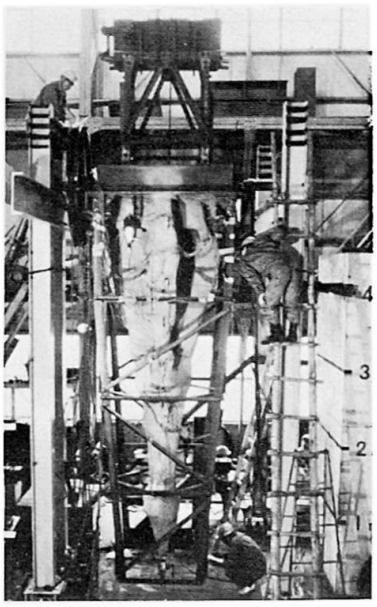

Fig. 6

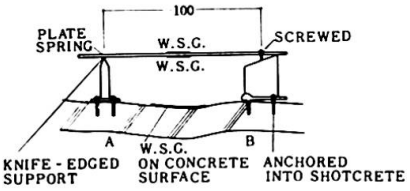

Fig. 7 Curvature Measurement Instrument

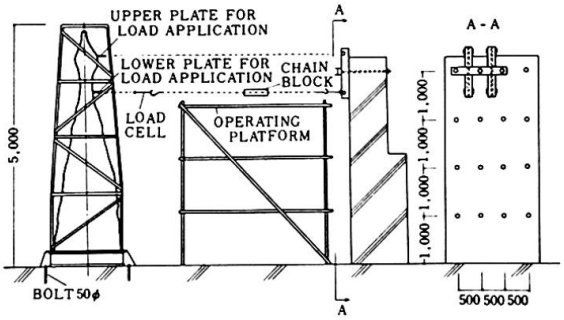

Fig. 8 Concentrated Loading Apparatus

4. Test Results

No cracks whatsoever were caused to the models by the load-by-gravity tests. Fig. 9 shows the load-deflection curves for these tests. It was generally found that the force normal to the axis of the tower (expressed $K = \sin\theta$, where θ = rotation angle) and the deflection were in a linear relationship; however, some decrease of rigidity was observed when the rotation angle approached $\theta = \pi/2$. Table 5 shows the results of studies on the initial rigidity values as observed at Points 1, 2 and 3 during the tests. In the table, the theoretical rigidity values for the case where the model was assumed to be a solid cantilever having the moments of inertia equal to those of the various horizontal sectional areas were taken as 1. Further, the theoretical values for the case where steel frame alone was considered effective are shown in Column 1 and the foregoing values modified by considering the curvature variation of the outer crust as will be discussed later are shown in Column 2 of the table. Column 3 of the same table shows the measured rigidity values.

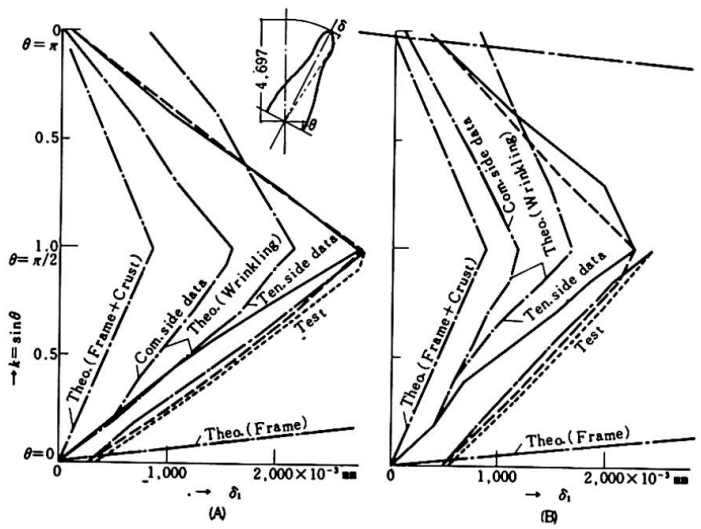

Fig. 9 Load-Deflection Curve

Table 5. Rigidity Ratio

The rigidity of the solid cantilever as described in Para. 5 being taken as unity.

		Model A			Model B		
	Measuring points	1	2	3	1	2	3
1	Rigidity ratio where steel frame only is effective	0.057	0.089	0.123	0.049	0.058	0.096
2	Rigidity ratio where the local bending of crust is taken into account in analysis	0.47	0.47	0.40	0.64	0.64	0.63
3	Rigidity ratio based on initial values obtained by tests	0.34	0.33	0.33	0.46	0.47	0.50

If the theoretical rigidity value of the solid cantilever was taken as 100%, the measured values for Model A and Model B were 33% and 50% respectively. It is believed that the initial rigidities as observed during the experiments are fairly well accounted for by the modified values shown in Column 2 of the table. The deformations at the apex of the models were 2.40 mm for Model A and 2.14 mm for Model B.

Fig. 10 shows the load-deflection curves; Table 6, the initial rigidity ratios of models; and Table 7, yield strength, ultimate strength and corresponding deformations; all for concentrated loading tests.

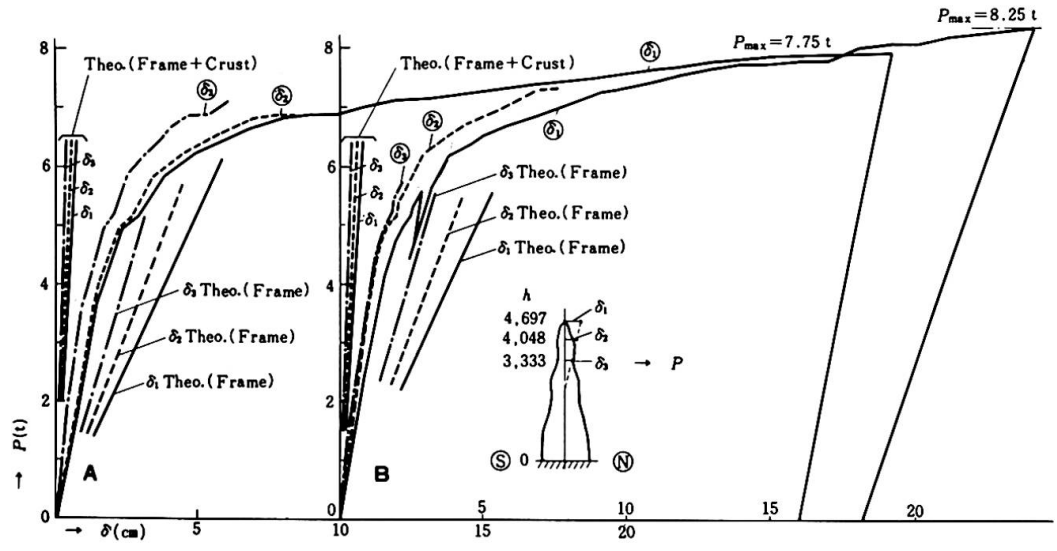

Fig. 10 Load-Deflection Curve

Table 6. Rigidity Ratio

The rigidity of the solid cantilever as described in Para.5 being taken as unity.

		Model A				Model B			
Measuring points		1	2	3	Mean	1	2	3	Mean
Initial rigidity by tests	Loading or upper part	0.23	0.19	0.30	0.24	0.27	0.30	0.34	0.30
Rigidity	Loading on lower part	0.32	0.31	0.29	0.31	0.56	0.21	0.44	0.40

Table 7. Permissible Load Bearing Capacity Proved by Tests

	Points of Load Application	Permissible load (R = 1/200)		Permissible load (R = 1/100)		Permissible load (Max)	
		Py(t)	δ top (cm)	Py'(t)	δ top (cm)	P max(t)	δ top (cm)
Model A	Upper part	1.5	2.5	2.08	5.0	2.17	6.1 (1/79)
	Lower part	5.0	2.5	6.2	5.0	7.75	30 (1/16)
Model B	Upper part	1.86	2.5	-	-	2.68	4.8 (1/100)
	Lower part	5.15	2.5	6.5	5.0	8.25	24 (1/20)

Values in ( ) represent joint translation angles.

Table 8. Permissible Load Bearing Capacity Proved by Analysis
(up to Level 1.965 m)

	Yield point of column / Yield point of shaft	Yield point of column / Strength of shaft	Strength of column / Yield point of shaft	Strength of column / Strength of shaft
Permissible Load	5.82 t (A 0.75) (B 0.71)	6.75 t (A 0.87) (B 0.82)	8.15 t (A 1.05) (B 0.99)	9.10 t

Values in ( ) represent $\frac{\text{Value resulting from analysis}}{\text{Theoretical value}}$

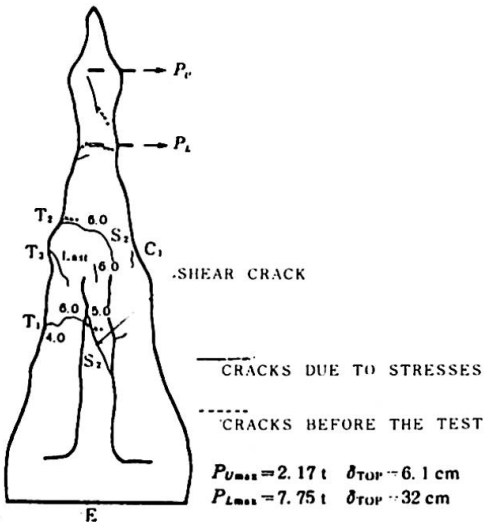

Fig. 11 Cracks Caused by the Concentrated Loading Test

A few examples are indicated in Fig. 11 to show how cracks appeared in the shotcreted crusts of the models. Some cracks had already took place prior to the tests because of the shrinkage due to drying. The cracks due to stresses in shotcrete were first caused by the shrinkage on the tensile side. They were followed by the vertical cracks and crushing on the compressive side at the next stage, and by the shear cracks at the ultimate stage.

Where the load was applied to the upper part of the model, the strength was governed by the shear resistance of the shotcrete at the point of load application. Where the load was applied to the lower part, the buckling of the steel column in compression located between the diaphragms was the governing factor. The different structural behaviours under the loads applied to different points of models resulted in the difference in permissible strengths shown in Table 7. In Table 8, the sums of the load bearing capacity of steel columns and that of central shaft, both as obtained by the analysis for the case where the load was applied to the lower part of the model, are compared with the corresponding load bearing capacity as obtained by the tests. The bearing capacity referred to above was taken as being equal to the yield point or strength of the material. For the central shaft, however, a certain elasto-plastic coefficient was assumed, and the bearing capacity contributed by the columns was computed on the assumption that the lever arm was equal to the spacing of the columns. It may be induced from the table that the steel members partially entered a state of strain hardening, and the shotcreted elements also contributed to increase the bearing capacity on the compressive side.

5. Deformation of Shotcrete Crust and Its Effects on Tower Structure Deflection

Fig. 12 indicates the relationship between the loads and the curvature variations due to stresses in shotcreted elements.

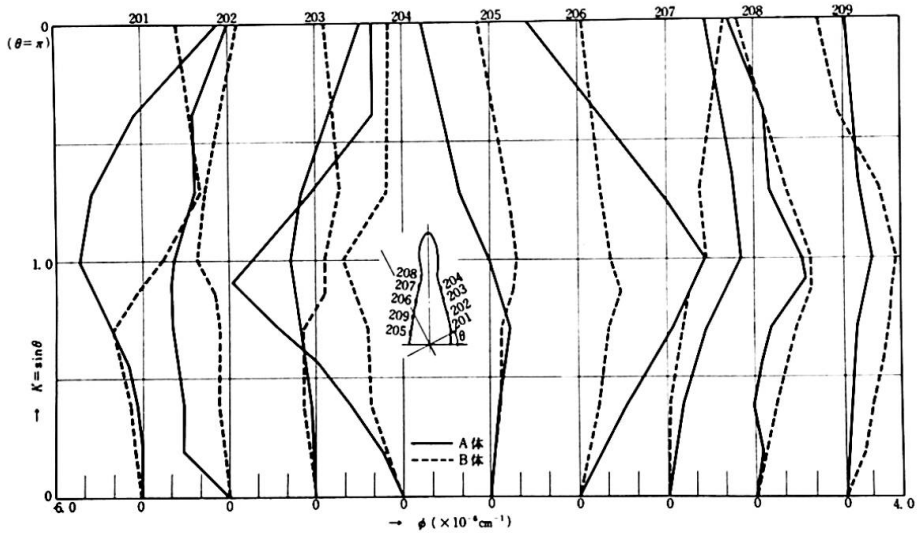

Fig. 12 Load-Curvature Curve

It is assumed that the overall deflection of the tower is a summation of (1) and (2) described below:

(1) Deflection of an imaginary solid cantilever beam in which shotcreted crust is fully integrated with steel frame. The solid cantilever beam is assumed to have the moments of inertia equal to those of the various cross sections involved.

(2) Deflection caused by the local bending of the shotcrete crust located on compressive and tensile extreme fibres of the tower structure. Because of the surface irregularities along the generating line of the tower shaft, this type of deflection was taken into account.

For Type (2) deflection, the analyses have been made as follows:
The part (approx. 10 cm in length) for which the curvature due to stresses in shotcrete crust was measured was assumed to form an arc-shaped section. If

the length of this arc, the length of the corresponding chord and the curvature after deformation are expressed as ℓ , χ and ϕ (where ϕ = the original curvature ϕ_0 + the curvature variation due to stresses $\Delta\phi$) respectively, then,

$$\chi = 2\frac{\sin(\frac{\ell}{2}\cdot\phi)}{\phi} \quad \cdots\cdots (5.1)$$

If it is further assumed that the change of ℓ does not give any influence on the deflection caused by the bending of shotcreted elements described in (2), then ℓ may be considered constant in Equation (5.1). From this equation, the variations of chord length χ can be obtained in proportion to the measured curvature variations $\Delta\phi$ caused by the stresses in rigid shotcreted elements. By adopting the expression that,

$$X = \chi/\chi_0 \ , \quad \Phi = \phi/\phi_0$$

(where χ_0 and ϕ_0 represent the chord length and curvature prior to deformation.)
the following equation can be written:

$$X = \frac{\sin(\frac{\ell}{2}\phi_0\Phi)}{\Phi\sin(\frac{\ell}{2}\phi_0)} \quad \cdots\cdots (5.2)$$

The increase of X expressed as $\Delta X (=\Delta\chi/\chi_0)$ resulting from the increase of Φ expressed as $\Delta\Phi (=\Delta\phi/\phi_0)$ can then be written as follows provided that $\Delta\Phi$ is very small:

$$\Delta X = \left(\frac{dX}{d\Phi}\right)_{\Phi=1}\cdot\Delta\Phi$$

$$\therefore \Delta X = \left(\frac{\ell}{2}\phi_0\cot\frac{\ell}{2}\phi_0 - 1\right)\cdot\Delta\Phi \quad \cdots\cdots (5.3)$$

And from the measurement results, we have,

$$|\Delta\Phi| \leq 0.046 \quad \cdots\cdots (5.4)$$

It should be noted that ΔX in Equation (5.3) corresponds to the strains at the tensile and compressive extreme fibres with regard to the plane perpendicular to the axis of the tower. The ΔX referred to above, however, was modified by multiplying it by the cosine corresponding to the axis of the tower at the points where measurement was taken.

The values of curvature for the tower as a whole were obtained by linear interpolation for the part in between the measuring points whereas the values obtained at the nearest measuring points were adopted without modification for the apex and base outside the measuring points.

The results of analyses so far described are plotted on Fig. 9 and Table 5. In case of Model A, the load-deflection curves as obtained from the analyses, the theoretical curves in which $\theta = 0 \sim \pi/16$ and coefficient of seismic force $k = 0 - 0.2$ coincide well with the measured curves until the coefficient k reaches 0.5 approximately at which value the measured curves begin to show the decrease of rigidity. In case of Model B, the curves for theoretical values coincide well with those for measured values until the seismic coefficient reaches 0.4 or so where the rigidity begins to decrease as can be observed from the curves for measured values. Unlike Model A, it is noticed in Model B that the theoretical curves show smaller deflections than measured curves for the same coefficient. The values shown at the column 3 of Table 5 are the arithmetical means of the theoretical values computed for the compressive side and those computed for the tensile side, both at the point where $k = 1.0$ and $\theta = \pi/2$.

6. Reflection of Test Results on the Design

A micro-vibration test conducted with a pick-up placed at Measurement Point 2 indicated the primary natural period of T_1 = 0.080 sec and the damping constant of h = 2% for Model A. The corresponding values for Model B were T_1 = 0.079 sec and h = 2.8%, as shown in Table 9.

Table 9. Vibration Test Results
(at Measuring Point 2)

		Before load application	After the upper part was loaded to failure of the model	After the lower part was loaded to failure of the model
Model A	T_1	0.080 sec	0.083 sec	0.092 sec
	h	2.0 %	2.3 %	0.64 %
Model B	T_1	0.079 sec	0.084 sec	0.103 sec
	h	2.8 %	1.8 %	0.68 %

T_1 : fundamental period (sec) h : damping coefficient (%)
Pick up period = 1 sec

In the load-by-gravity tests where the maximum deflection at the apex was y cm, the values of c at T = $\sqrt{y}$ /c were 6.1 and 5.9 for Model A and Model B respectively. When the theoretical value T_1 = 0.95 sec as computed on the assumption that the tower was a solid cantilever beam was compensated by a factor for initial rigidity decrease, then T_1 = 1.66 sec and T_1 = 1.40 sec were obtained for Model A and Model B respectively.

As it became possible to predict the characteristics of vibration and the mechanism of rupture of the actual tower, the natural period and damping coefficient were assumed by reference to the values obtained by the experiment, and the tower's response to various pattern of earthquake waves was computed for analysis to provide the data on which to base the cross sections at the final design stage. As for the effects of external forces, earthquakes rather than wind loads were found to give greater influence, and consequently seismic resistance became the primary design consideration. The measured periods of actual tower under the influence of micro-tremors were found to be 1.82 sec (h = 0.6%) for the fundamental mode of vibration. The similar values for the secondary and the tertiary modes were 0.6 sec and 0.31 respectively.

7. Conclusions

The major findings observed in the experiments using 1/33 scale models may be summarized as follows:

(1) Despite an unprecedented testing method employed for the load-by-gravity tests, the experiment was carried out without encountering much difficulty.

(2) The rigidity of the models subjected to the load-by-gravity tests was found to have the values intermediate between the rigidity of the structure in which shotcreted crust and steel frame are considered fully integrated to form effective sectional area and the rigidity of structure for which steel frame only forms effective sectional area. The measured rigidity of Model A was approximately 1/3 of the value which would have been obtained if the entire combined sections had been effective. This relative value was about 1/2 in case of Model B which had a thicker crust. A similar tendency was observed during the concentrated tests from which it was found that the values of initial rigidity were about 1/4 - 1/3 and about 1/3 - 1/2 for Model A and Model B respectively. The rigidity values thus made predictable from the experiments were considered reasonably accurate to serve the

purpose of the structural design which ensued.

(3) In the concentrated loading tests, the load-bearing capacity of the model loaded at the upper part was governed by the shear resistance of the shotcrete at the point to which the load was applied whereas the capacity was governed by the buckling of the steel in compression in case the load was applied to the lower part. The deflection of the apexes of the models reached 1/16 - 1/20 in these cases, which was considered indicative of sufficient ductility.

(4) The natural periods of the models tended to prolong as the fracture progressed. This tendency was considered due to the decrease of rigidity. On the contrary, the damping constant tended to decrease as the fracture progressed.

(5) When the rigidity of shotcrete was taken into account based on technological evaluation of the test results in order to simulate vibration models for analysis, the fundamental period and damping constant became 1.84 and 2% respectively.

(6) The tower was constructed to the design which was based on the results of these experiments. The natural period of the actual tower under micro tremors was observed and found to coincide well with that of the models.

Summary

In order to obtain the data for earthquake-resistant design of a 170 m high sculptural tower composed of steel frames and shotcreted crust, loading tests were conducted on 1/33 scale models. For the loading tests, the models were fixed at the base and turned up and down. Thus, the members involved were subjected to lateral forces proportional to their weight nearly in the same way as they would be under earthquakes. It was indicated by these experiments that the rigidity of models could be accounted for by taking into consideration the local bending of shotcrete. The tests also helped to clarify the structural behaviours under ultimate loads. The experiments served their intended purposes satisfactorily as the test results were in many ways reflected in the final design.

Bibliography

Research study on the seismic resistance of PL Peace Tower, by H. Tada and Y. Sonobe, Synopses of Transactions, Architectural Institute of Japan, November 1971.

PL Peace Tower, edited by Nikken Sekkei Ltd, Geijutsu Seikatsu Sha, August 1970.

V

Evaluation of Gusts on Flexible Structures

Estimation des efforts dynamiques aux structures souples

Abschätzung der Einwirkung von Stössen auf flexible Bauwerke

TOSHIO MIYATA
Lecturer

MANABU ITO
Associate Professor

Department of Civil Engineering
Faculty of Engineering
University of Tokyo, Japan

Introduction

The contribution described herein forms part of a study of the gust responses of flexible structures such as long-spanned bridges, tall-slender buildings and towers. Dynamic excitation of structures by wind action can usually referred to the following causes: (1) instability of the galloping, stall flutter and (classical) flutter types, (2) buffetting by vortices and turbulence shed in the wake of the structure, (3) buffetting by gusts and (4) buffetting by vortices shed by the other surrounding structures. These causes are possible either together or separately.

The indication of criteria for the determination of the effects of gusts have been so far considered, in the form of gust factor *1*), *2*), with regard to the oscillation of mean wind direction (drag component), and a number of other factor have not been so much investigated owing to the difficulty of generalization. They could, however, be indispensable, for instance, when there is a possibility of negative aerodynamic damping. Many common structural shapes have usually a potential of instability at certain critical wind velocities. Such structural shapes as square, rectangular and H-shaped sections, plate girder bridges, truss bridges and streamlined sections are those with which aerodynamic instability or vortex excitation has been known to occur.

In this paper it is indicated that the dynamic effects of gusts on items except (4) described above are generally expressed by using unsteady aerodynamic forces obtained experimentally or theoretically, and a couple of illustrative examples are presented in the calculation of gust responses of particular structural cases.

Formulation of Gust Responses

The proper recognition of the dynamic effects of wind in conjunction with design wind velocity estimates depends on the prediction of the statistical distribution of the responses of the structure--stress, deflection or local pressure. To derive these distributions it is well known that two types of information are required with the distribution of reference wind velocities

observed at the site of the structure and the aerodynamic responses based on a certain reference wind velocity. The reference wind velocity and the structure of the wind are assumed to be already known in the following discussion.

In smooth flow the unsteady aerodynamic forces acting on a two-dimensional body oscillating with displacements of lift motion $Z(t)$ and pitching moment motion $\phi(t)$ at circular frequency ω are expressed as:
for the lift force,

$$L = \pi\rho\left(\frac{B}{2}\right)^3\omega^2\left[\left(L_{ZR} + iL_{ZI}\right)\frac{Z}{B/2} + \left(L_{\phi R} + iL_{\phi I}\right)\phi\right]$$

and for the pitching moment, (1)

$$M = \pi\rho\left(\frac{B}{2}\right)^4\omega^2\left[\left(M_{ZR} + iM_{ZI}\right)\frac{Z}{B/2} + \left(M_{\phi R} + iM_{\phi I}\right)\phi\right]$$

where $i = \sqrt{-1}$, ρ is air density, B is the width of the body in the wind direction and the unsteady aerodynamic coefficients L_{ZR}, L_{ZI}, ... and $M_{\phi I}$ are real functions of reduced frequency

$$\xi = \frac{n\,B}{U} = \frac{1}{\pi}\left(\frac{\omega\,B}{2\,U}\right) \tag{2}$$

at wind velocity U and frequency n. The only theoretical analysis for the unsteady aerodynamic coefficients have been derived for a flat plate section as follows:

$$\begin{aligned} L_Z &= L_{ZR} + iL_{ZI} = -\frac{2i}{\pi\xi}C(\pi\xi),\quad L_\phi = L_{\phi R} + iL_{\phi I} = -\frac{2}{(\pi\xi)^2}C(\pi\xi) - \frac{i}{\pi\xi}[1 + C(\pi\xi)] \\ M_Z &= M_{ZR} + iM_{ZI} = \frac{i}{\pi\xi}C(\pi\xi),\quad M_\phi = M_{\phi R} + iM_{\phi I} = \frac{1}{(\pi\xi)^2}C(\pi\xi) - \frac{i}{2\pi\xi}[1 - C(\pi\xi)] \end{aligned} \tag{3}$$

in which $C(\pi\xi) = F(\pi\xi) + iG(\pi\xi)$ is a complex Theodorsen function 3). As far as structural shapes described above are concerned, generally speaking, it is difficult to derive these unsteady aerodynamic coefficients analytically, and there is no way to derive other than experimental measurements. The measured coefficients are given in Fig. 1 for a couple of sections 4) together with a flat plate section. The measuring experiments were carried out by a so-called forced oscillation method, in which the unsteady coefficients are obtained by giving a body forced oscillations with constant amplitude and frequency as a parameter of ξ.

In turbulent flow with mean wind velocity $\overline{U}$ and fluctuating velocity components of along wind u and cross wind w (vertical) or v (lateral), the aerodynamic forces that act on a body are partly due to the fluctuating components of turbulent flow and partly due to the motion of the body itself, that is, part of unsteady aerodynamic forces. The latter part must, strictly speaking, be different from that in smooth flow. Thus, the aerodynamic forces can be expressed in turbulent flow as:

$$\begin{aligned} L^* &= \pi\rho\left(\frac{B}{2}\right)^3\omega^2\left[\left(L_{ZR}^* + iL_{ZI}^*\right)\frac{Z}{B/2} + \left(L_{\phi R}^* + iL_{\phi I}^*\right)\phi\right] + L_f(t) \\ M^* &= \pi\rho\left(\frac{B}{2}\right)^4\omega^2\left[\left(M_{ZR}^* + iM_{ZI}^*\right)\frac{Z}{B/2} + \left(M_{\phi R}^* + iM_{\phi I}^*\right)\phi\right] + M_f(t) \end{aligned} \tag{4}$$

in which the reduced frequency $\xi = \frac{1}{\pi}\left(\frac{\omega B}{2U}\right)$. Whether or not the forces induced by above two parts are linearly superposable will be a question requiring further attention in the understanding of the identification of each part and the complex

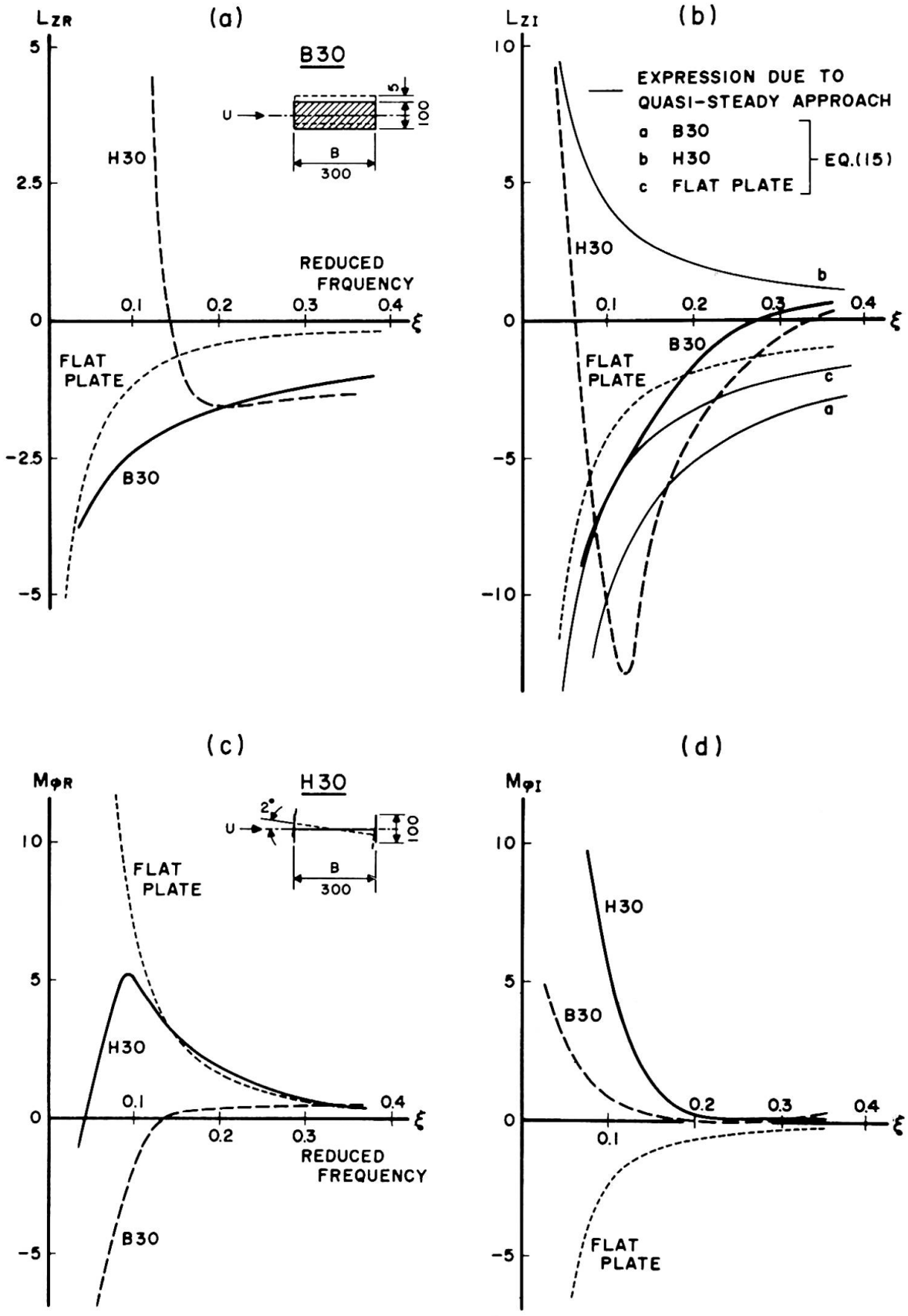

Fig. 1 EXAMPLES OF MEASURED AERODYNAMIC COEFFICIENTS FOR LIFT AND MOMENT RESPONSES OF RECTANGULAR AND H-SHAPED SECTIONS TOGETHER WITH THEORETICAL ONES OF FLAT PLATE SECTION

interaction between the turbulence in the approaching flow and the wake generated by the oscillatory body. Each coefficients of eq. (4) is available in principle by the same forced oscillation method as in smooth flow, if the turbulent flow in wind tunnel is well simulated to the natural wind.

It can be seen that the justification of the separation into two independent parts and the superposition of them in eq. (4) depends on the assumption of small disturbances. Then, as the first approximation, the expression of eq. (4) may be valid and the replacement of coefficients L_{ZR}^*, L_{ZI}^*, ... and $M_{\phi I}^*$ by L_{ZR}, L_{ZI}, ... and $M_{\phi I}$ in smooth flow can be assumed for turbulence of small intensity.

Including several kinds of oscillations such as vertical one of bridges due to vertical components of turbulence, lateral one of tall-slender structures transverse to the mean wind direction caused by lateral components of turbulence as well as oscillations of the mean wind direction caused by longitudinal components, the gust responses of flexible structures to atmospheric turbulence can be expressed as in the following discussion by means of such the aerodynamic forces as given in eq. (4). All the aerodynamic characteristics of structural shapes, whether the section is stable or there is a possibility of negative aerodynamic damping, should be represented in the forms of unsteady aerodynamic forces.

Let us consider an illustrative analysis of vertical responses to vertical components w of turbulent flows of a system that has coupled oscillation characteristics with vertical and torsional motions. The spectrum $S_Z(x;\ n)$ of the displacement $Z(x;\ t)$ at a point x of the span in the rth mode can be expressed by

$$S_Z(x;\ n) = S_w(n)\ |X_L(n)|^2\ |J_w(n)|^2\ |X_Z(x;\ n)|^2 \tag{5}$$

in which $S_w(n)$ is the spectrum of vertical component w of turbulence, $|X_L(n)|$ the frequency response (admittance) of the lift to a sinusoidal gust w, $|X_Z(x;\ n)|$ the frequency response of the displacement to a sinusoidal lift force, and $|J_w(n)|^2$ named the joint acceptance.

As to the frequency response of the displacement to a sinusoidal lift force, it can be obtained by examining the dynamic solution of the system subjected to a harmonic exciting lift $L_f(t) = L_o e^{iwt}$ at $x = x_L$. Using the expressions of eqs. (1) and (4) and letting $M_f(t) = 0$, the equations of motion are:

$$\begin{aligned} m\ [\ddot{Z} + i \cdot 2\zeta_1\omega_1\dot{Z} + \omega_1{}^2 Z] - L &= L_f \\ \theta\ [\ddot{\phi} + i \cdot 2\zeta_2\omega_2\dot{\phi} + \omega_2{}^2\phi] - M &= 0 \end{aligned} \tag{6}$$

where m and θ are the mass and the polar moment of inertia per unit length, ζ_1 and ζ_2 the mechanical damping ratio, and ω_1 and ω_2 the circular natural frequency in vertical and torsional motions, respectively. The solution is

$$Z(x;\ t) = \frac{L_o e^{iwt}}{\pi\rho(B/2)^2\omega^2} \frac{A_4}{\begin{vmatrix} A_1 & A_2 \\ A_3 & A_4 \end{vmatrix}} \frac{\phi(x)\phi(x_L)}{\int_o^l \phi^2(x)dx} \tag{6a}$$

in which $\phi(x)$ is the rth mode shape, l the span length and

$$A_1 = \mu[-1 + i\cdot 2\zeta_1\frac{\omega_1}{\omega} + (\frac{\omega_1}{\omega})^2] - (L_{ZR} + iL_{ZI}),\quad A_2 = -(L_{\phi R} + iL_{\phi I})$$
$$A_3 = -(M_{ZR} + iM_{ZI}),\quad A_4 = \nu[-1 + i\cdot 2\zeta_2\frac{\omega_2}{\omega} + (\frac{\omega_2}{\omega})^2] - (M_{\phi R} + iM_{\phi I}) \tag{6b}$$

$$\mu = \frac{m}{\pi\rho(B/2)^2},\qquad \nu = \frac{\theta}{\pi\rho(B/2)^4} \tag{6c}$$

The quantity $|X_Z(x;\ n)|$ is, therefore, derived as

$$|X_Z(x;\ n)| = \frac{\phi(x)}{\pi\rho(B/2)^2\omega^2}\frac{A_4}{\begin{vmatrix} A_1 & A_2 \\ A_3 & A_4 \end{vmatrix}} \tag{7}$$

which differs from the familiar resonance curve of the mechanical admittance, and the joint acceptance is expressed by

$$|J_w(n)|^2 = \int_o^l\int_o^l \phi(x_1)\phi(x_2)R_w(x_1,\ x_2;\ n)dx_1dx_2\ /\ [\int_o^l \phi^2(x)dx]^2 \tag{8}$$

in which $R_w(x_1,\ x_2;\ n)$ is the spanwise cross correlation of w at points x_1 and x_2 and at frequency n.

The lift force caused by vertical component w of turbulence, that is, $L_f(t)$ in eq. (4) may be approximately given in the form:

$$L_f(t) = \frac{1}{2}\rho B(\frac{dC_L}{d\alpha})\overline{U}^2\cdot\frac{w(t)}{\overline{U}}X_w(\xi) \tag{9}$$

in which $X_w(\xi)$ is the term corresponding to the frequency response (aerodynamic admittance) of the lift to gust w, and $dC_L/d\alpha$ the rate of change of steady lift coefficient with flow inclination α. Vickery *5*) has investigated the drag force/velocity relationship for bluff prismatic structures of low aspect ratio, being in a reasonable agreement with theoretical estimates based on a lattice structure. Bearman *6*) has also examined the relationship between the approaching turbulent flow and the mean and fluctuating forces on a series of flat plates set normal to the flow. It was concluded that at values of $\xi = nB/U$ less than 0.1 the drag/velocity relationship helped to justify the concept of aerodynamic admittance, but the measurements suggested, at high values of ξ, a further contribution to drag fluctuations, uncorrelated with upstream velocity, perhaps resulting from wake-induced fluctuations on the rear face, although the level of the spectra in turbulent flow was three orders greater than in smooth flow at the same value of ξ. This may suggest that it is significant to use unsteady aerodynamic forces in evaluating the gust responses.

Sears *3*) has shown the expression, for a flat plate section, in the form

$$L_f(t) = \frac{1}{2}\rho B(2\pi)\overline{U}^2\cdot\frac{w_o e^{iwt}}{\overline{U}}X_w(\xi) \tag{9a}$$

and the approximation of $X_w(\xi)$ has been given by Liepmann *3*) as follows:

$$|X_w(\xi)|^2 = \frac{1}{1 + 2\pi^2\xi} \tag{10}$$

The frequency response (admittance), in eq. (5), therefore, is presented as

$$|X_L(n)| = \pi\rho B\bar{U}\ |X_w(\xi)| \tag{11}$$

If the response is limited to one degree of freedom, the expressions of the frequency response of the displacement to a sinusoidal exciting force are rewritten in simpler forms. For the combination of translational (vertical or lateral) displacement and lift force,

$$|X_Z(x;\ n)|^2 \quad \text{or} \quad |X_x(Z;\ n)|^2 = \frac{\phi^2(x)}{16\pi^4 m^2 n_o^4} \frac{1}{[1 - (\frac{n}{n_o})^2 - (\frac{n}{n_o})^2\frac{L_R}{\mu}]^2 + [2\zeta_o\frac{n}{n_o} - (\frac{n}{n_o})^2\frac{L_I}{\mu}]^2} \tag{12a}$$

in which L_R and L_I are real and imaginary unsteady aerodynamic force components due to translational displacement respectively, n_o the natural frequency and ζ_o the mechanical damping ratio, and for torsional displacement,

$$|X_\phi(x;\ n)|^2 = \frac{\phi^2(x)}{16\pi^4\theta^2 n_2^4} \frac{1}{[1 - (\frac{n}{n_2})^2 - (\frac{n}{n_2})^2\frac{M_{\phi R}}{\nu}]^2 + [2\zeta_2\frac{n}{n_2} - (\frac{n}{n_2})^2\frac{M_{\phi I}}{\nu}]^2} \tag{12b}$$

The same expression as in eq. (12a) is also possible with the drag response of the mean wind direction, provided the aerodynamic coefficients are available by measuring each component of unsteady drag force giving the body an along-wind oscillation.

The coefficients such as L_{ZI} and $M_{\phi I}$ indicate the effects of aerodynamic damping (or exciting), because the imaginary terms are correlated with phase lag between displacement and force acting on the body. The aerodynamic damping (or exciting) ratio can be derived from the quasi-steady approach as well. Davenport *7*) has shown the logarithmic decrements for drag direction responses

$$\delta_p = \frac{\bar{P}}{n_o\bar{U}m} \tag{13a}$$

and for translational responses

$$\delta_L = \frac{d\bar{L}/d\alpha}{2n_o\bar{U}m} \tag{13b}$$

in which $\bar{P} = \frac{1}{2}\rho B\bar{U}^2 C_D$, $\bar{L} = \frac{1}{2}\rho B\bar{U}^2 C_L$ and C_D and C_L are steady drag and lift coefficients. The term in eq. (12a) associated with damping is rewritten as

$$2\zeta_o\frac{n}{n_o} - (\frac{n}{n_o})^2\frac{L_I}{\mu} = 2\frac{n}{n_o}(\zeta_o - \frac{n}{n_o}\frac{L_I}{2\mu})$$

and, thus, the aerodynamic damping (or exciting) term is

$$\zeta_{aero} = -\frac{n}{n_o}\frac{L_I}{2\mu} \tag{14}$$

Combining eq. (13) and eq. (14), the expressions of L_1 due to quasi-steady approach are derived for translational responses and along-wind responses respectively:

$$P_I = -\frac{2C_D}{\pi^2}\frac{1}{\xi}, \qquad L_I = -\frac{dC_L/d\alpha}{\pi^2}\frac{1}{\xi} \tag{15}$$

Numerical Examples

Vertical Gust Responses of Flat Plate Section To find the vertical responses of a taut strip model of flat plate section to boundary layer turbulent flows, derive the root mean square of response from the results of $S_Z(x;\ n)$ in eq. (5).

$$\sigma_Z(x) = \sqrt{\int_0^\infty S_Z(x;\ n)dn} \tag{16}$$

The factor $X_Z(x;\ n)$, the frequency response of the displacement to a sinusoidal lift force can be computed according to eq. (7), using the aerodynamic coefficients in eq. (3) with regard to frequency n as a parameter of wind velocity. The results are shown in Fig. 2, which indicates that peak responses shift from a frequency close to the natural frequency to that close to the critical frequency with increase of wind velocity. Every dimension used in calculation is due to the work by Davenport, Isyumov and Miyata *8*) as follows:

l = 228.6 cm, B = 9.36 cm

μ = 11.1, ν = 2.26 from eq. (6c)

n_1/n_2 = 7.6/21.2 = 0.36

ζ_1 = 0.0024, ζ_2 = 0.01

The root-mean-square responses are, finally, obtained as indicated in Fig. 3 together with experimental results *8*). In the case of 9% of intensity of turbulence, the agreement of both is reasonably good.

Comparison of Aerodynamic Coefficients with Those due to Quasi-steady Approach As to the sections shown in Fig. 1, compute aerodynamic coefficients L_I due to eq. (15).

	$\{dC_L/d\alpha\}_{\alpha = 0°}$		L_I
B 30	9.98	} ref. *4*)	$-\frac{1.01}{\xi}$
H 30	-4.02		$\frac{0.407}{\xi}$
FLAT PLATE	2π		$-\frac{0.638}{\xi}$

The results are shown in Fig. 1(b) together with experimental values measured by the forced oscillation method. The agreement of both is poor with a slight exception of small values of ξ. On the other hand, in the case of drag responses of a truss bridge, it is likely that the expression of aerodynamic damping due to quasi-steady approach is comparatively reasonable. Fig. 4 shows a result of aerodynamic coefficients for lateral (drag) motions of a suspension bridge model. Dimensions of the truss bridge model are l = 16 m, B = 35.5 cm, m = 4.66 x 10^{-2} g sec^2/cm^2, n_o = 0.46 c/s and C_D = 0.29. For this case,

$$P_I = -\frac{2 \times 0.29}{\pi^2}\frac{1}{\xi} = -\frac{0.059}{\xi} \qquad \text{from eq. (15)}$$

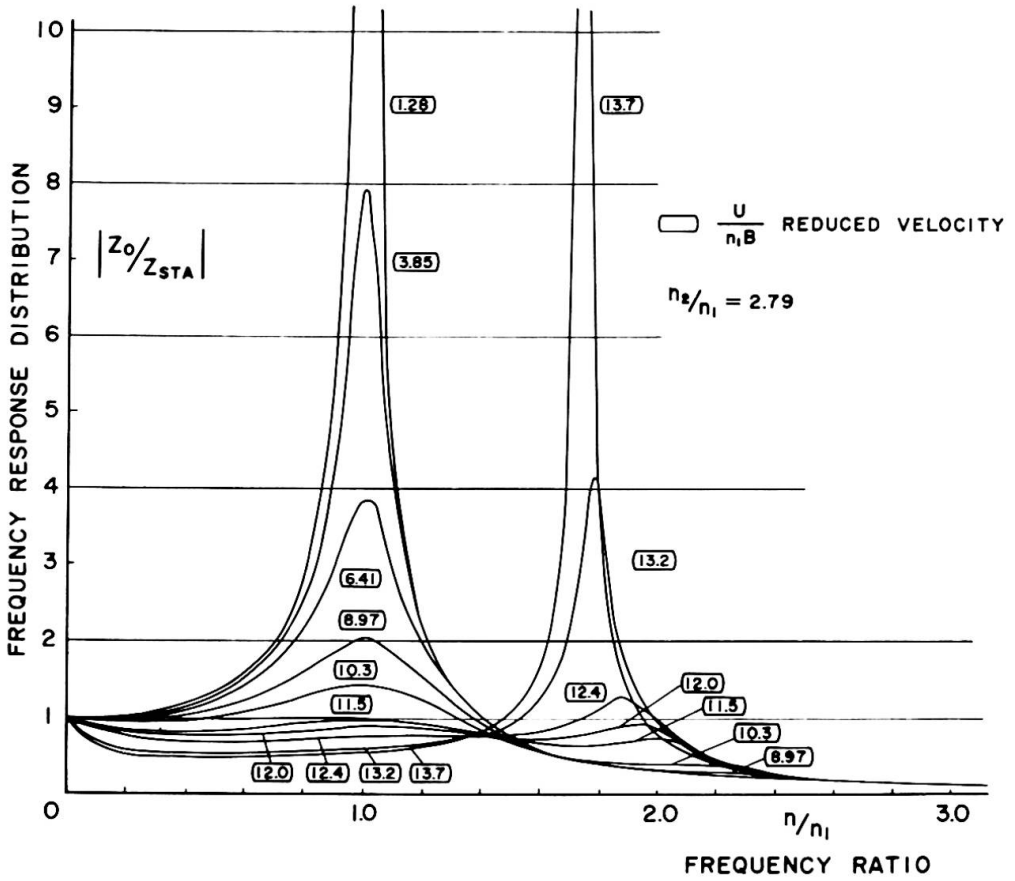

Fig. 2 FREQUENCY RESPONSE OF VERTICAL DISPLACEMENT $Z = Z_o e^{i\omega t}$ OF FLAT PLATE SUBJECTED TO SINUSOIDAL EXCITING LIFT FORCE $L_f = L_o e^{i\omega t}$

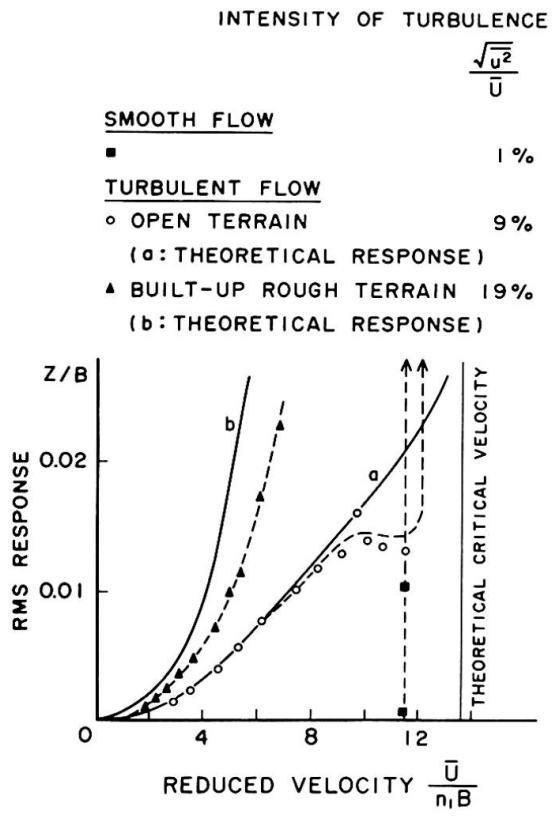

Fig. 3 VERTICAL GUST RESPONSES OF FLAT PLATE TAUT STRIP MODEL [ORIGINAL EXPERIMENTAL DATA DUE TO REFERENCE 8)]

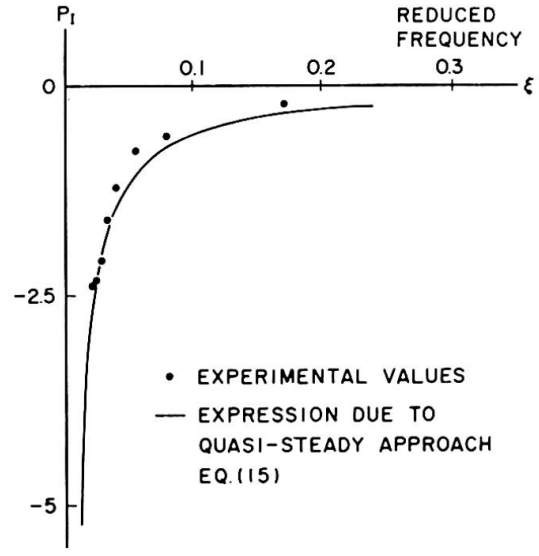

Fig. 4 AERODYNAMIC COEFFICIENT FOR ALONG-WIND (DRAG) RESPONSE OF TRUSS BRIDGE

Application to Along-Wind Gust Responses of Suspension Bridges It is well known that long-spanned suspension bridges are determined in designing due to the along-wind action of wind. The evaluation of gust responses of suspension bridges has been examined by Davenport *7*), and the statistical approach has been used in Japan *9*) to derive a factor to give the design wind velocity for the static action of gusts. According to Davenport's treatment, find the gust factor G for suspension bridges with center span length of 500-1500 m and truss stiffening girders. As parameters of calculation, assumed the height Z of stiffening girders and the reference wind velocity $\overline{U}_{10}$ (mean wind velocity averaged over 10 min. at Z = 10 m) appropriately. The wind conditions over open sea are chosen as follows:

wind velocity at Z; $\overline{U}_Z = (\frac{Z}{10})^{1/7}\overline{U}_{10}$, roughness coefficient K; 0.003

spanwise cross correlation of u; $R_u(x_1, x_2; n) = \exp(-\frac{7n}{\overline{U}_Z}|x_1 - x_2|)$

The mechanical damping $\delta_o = 0.03$ is assumed, and the aerodynamic damping effect is considered due to $P_I = -\frac{2C_D}{\pi}\frac{1}{\xi}$. The frequency response (aerodynamic admittance) of the drag to gust u is, due to Vickery's expression *2*),

$$|X_u(n)|^2 = \frac{1}{1 + 2(nD/\overline{U}_Z)^{4/3}} \tag{17}$$

Finally, the gust factor $G(x)$ to be computed is in the form of

$$G(x) = \sqrt{1 + g(x)\frac{\sigma_M(x)}{\overline{M}(x)}} \tag{18}$$

in which $g(x) = \sqrt{2\ell n[600\nu(x)]} + \frac{0.5772}{\sqrt{2\ell n[600\nu(x)]}}$; and $\overline{M}(x)$ is mean bending moment by mean wind load, $\sigma_M(x)$ the variance of bending moment by gusts and $\nu(x)$ the effective frequency. The results for a series of suspension bridges, of which the properties *10*) are chosen as follows, are given in Fig. 5.

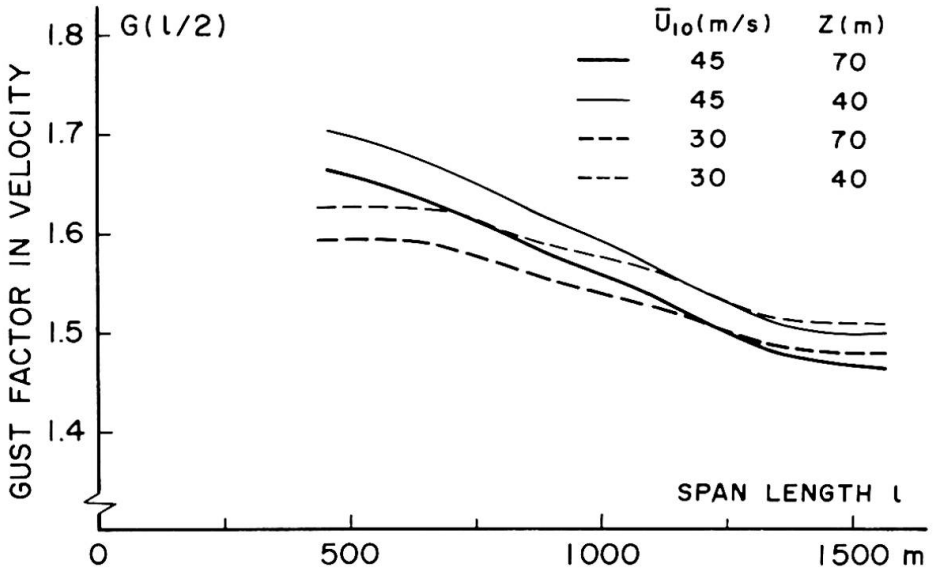

Fig. 5 GUST FACTOR IN WIND VELOCITY FOR ALONG-WIND (DRAG) RESPONSE - BENDING MOMENT - OF SUSPENSION BRIDGES

span length l	(m)	1500	1300	1000	800	650	500
width of truss B	(m)	36	36	33	33	33	33
height of girder D	(m)	14	14	11	11	8	8
sag dip	(m)	150	130	100	73	59	45
lateral rigidity $EI_h \times 10^{-9}$	(tm^2)	1.266	1.249	0.923	1.012	0.731	0.781
weight of truss w_t	(t/m)	20.28	20.05	19.32	19.66	19.01	19.01
weight of cables w_c	(t/m)	11.40	9.35	7.95	5.57	4.51	3.47
drag coefficient C_D		0.26	0.26	0.23	0.23	0.21	0.21
ratio of load (cables/truss)		0.261	0.233	0.214	0.184	0.167	0.148

References

1) Davenport, A. G., Gust Loading Factors, Proc. ASCE, Vol. 93, ST3, 1967.
2) Vellozzi, J. and Cohen, E., Gust Response Factors, Proc. ASCE, Vol. 94, ST6, 1968;
Vickery, B. J., discussion of Gust Response Factors by J. Vellozzi and E. Cohen, Proc. ASCE, Vol. 95, ST3, 1969.
3) Fung, Y. C., Theory of Aeroelasticity, John Wiley and Sons, 1955.
4) Tanaka, Hiroshi, The Characteristics of the Aerodynamic Forces in Self-Excited Oscillations of Bridge Structures (in Japanese), Dr. Dissertation submitted to University of Tokyo, Dec. 1968.
5) Vickery, B. J., Load Fluctuations in Turbulent Flow, Proc. ASCE, Vol. 94, EM1, 1968.
6) Bearman, P. W., An Investigation of the Forces on Flat Plates Normal to a Turbulent Flow, J. Fluid Mech., Vol. 46, Part 1, 1971.
7) Davenport, A. G., Buffetting of a Suspension Bridge by Storm Winds, Proc. ASCE, Vol. 88, ST3, 1962.
8) Davenport, A. G., Isyumov, N. and Miyata, T., The Experimental Determination of the Response of Suspension Bridges to Turbulent Wind, Proc. Third Int. Con. on Wind Effects on Buildings and Structures (Tokyo, Sept. 1971), 1972.
9) Hirai, A. and Okubo, T., On the Design Criteria against Wind Effects for Proposed Honshu-Shikoku Bridges, Proc. Int. Sym. on Suspension Bridges (Lisbon), Paper 10, 1966.
10) Ministry of Construction, Japan Government, Examination Report of Highways connecting Honshu and Shikoku (in Japanese), March 1970.

Summary

The gust responses of flexible structures are evaluated by taking into account unsteady aerodynamic forces due to the motion of the body itself. That is, under assumption of small intensity of turbulence, the aerodynamic forces are assumed to consist of the part due to the fluctuating components of turbulence and the unsteady part in smooth flow. As the unsteady aerodynamic force expression could include the effect of instability due to negative aerodynamic damping or vortex excitation phenomena as well, the general treatment of gust responses is probable. A couple of numerical examples show the validity of this concept.